

1 **Microbiome–host systems interactions: Protective effects of propionate upon**
2 **the blood–brain barrier**

3

4 Lesley Hoyles^{1*}, Tom Snelling¹, Umm-Kulthum Umlai¹, Jeremy K. Nicholson¹, Simon
5 R. Carding^{2, 3}, Robert C. Glen^{1, 4} & Simon McArthur^{5*}

6

7 ¹Division of Integrative Systems Medicine and Digestive Disease, Department of
8 Surgery and Cancer, Imperial College London, UK

9 ²Norwich Medical School, University of East Anglia, UK

10 ³The Gut Health and Food Safety Research Programme, The Quadram Institute,
11 Norwich Research Park, Norwich, UK

12 ⁴Centre for Molecular Informatics, Department of Chemistry, University of Cambridge,
13 Cambridge, UK

14 ⁵Institute of Dentistry, Barts & the London School of Medicine & Dentistry, Blizard
15 Institute, Queen Mary University of London, London, UK

16

17 ***Corresponding authors:** Lesley Hoyles, lesley.hoyles11@imperial.ac.uk; Simon
18 McArthur, s.mcarthur@qmul.ac.uk

19 **Running title:** Propionate affects the blood–brain barrier

20 **Abbreviations:** ADHD, attention-deficit hyperactivity disorder; ASD, autism spectrum
21 disorder; BBB, blood–brain barrier; CNS, central nervous system; FFAR, free fatty acid
22 receptor; KEGG, Kyoto Encyclopaedia of Genes and Genomes; GO, Gene Ontology;

23 LPS, lipopolysaccharide; SCFA, short-chain fatty acid; SPIA, Signalling Pathway
24 Impact Analysis.

25

26 **Abstract**

27 Background: Gut microbiota composition and function are symbiotically linked with
28 host health, and altered in metabolic, inflammatory and neurodegenerative disorders.
29 Three recognized mechanisms exist by which the microbiome influences the gut–brain
30 axis: modification of autonomic/sensorimotor connections, immune activation, and
31 neuroendocrine pathway regulation. We hypothesized interactions between circulating
32 gut-derived microbial metabolites and the blood–brain barrier (BBB) also contribute to
33 the gut–brain axis. Propionate, produced from dietary substrates by colonic bacteria,
34 stimulates intestinal gluconeogenesis and is associated with reduced stress
35 behaviours, but its potential endocrine role has not been addressed.

36 Results: After demonstrating expression of the propionate receptor FFAR3 on human
37 brain endothelium, we examined the impact of a physiologically relevant propionate
38 concentration (1 μ M) on BBB properties *in vitro*. Propionate inhibited pathways
39 associated with non-specific microbial infections via a CD14-dependent mechanism,
40 suppressed expression of LRP-1 and protected the BBB from oxidative stress via
41 NRF2 (NFE2L2) signaling.

42 Conclusions: Together, these results suggest gut-derived microbial metabolites
43 interact with the BBB, representing a fourth facet of the gut–brain axis that warrants
44 further attention.

45

46

47

48 **Background**

49

50 The human body plays host to, and exists in symbiosis with, a significant number of
51 microbial communities, including those of the skin, oral and vaginal mucosae and, most
52 prominently, the gut [1]. This relationship extends beyond simple commensalism to
53 represent a major regulatory influence in health and disease, with changes in
54 abundance of members of the faecal microbiota having been associated with numerous
55 pathologies, including diabetes, hepatic diseases, inflammatory bowel disease, viral
56 infections and neurodegenerative disorders [2–8]. Metagenomic studies have revealed
57 reductions in microbial gene richness and changes in functional capabilities of the faecal
58 microbiota to be signatures of obesity, liver disease and type II diabetes, and that these
59 can be modified by dietary interventions [9,10]. The gut microbiome harbours 150 times
60 more genes than the human genome, significantly increasing the repertoire of functional
61 genes available to the host and contributing to the harvesting of energy from food [11].

62

63 The primary form of communication within the gut microbe–human super-system is
64 metabolic, but our understanding of the details of the cross-signalling pathways involved
65 is limited. It is clear, however, that gut-derived microbial metabolites and products such
66 as lipopolysaccharide (LPS) can influence human health both in the intestine and
67 systemically [12,13], with reported effects ranging from mediation of xenobiotic toxicity
68 [14], through modification of the risk of preterm birth [15] to induction of epigenetic
69 programming in multiple host tissues [16,17]. A major aspect of microbe–host systems-
70 level communication that is receiving increased attention is the influence the gut
71 microbiota exerts upon the central nervous system (CNS), the so-called ‘gut–brain axis’
72 [18].

73

74 The existence of gut–brain communication is supported by a number of animal and
75 human studies, although the underlying mechanisms are not always well defined.
76 Behavioural analysis of antibiotic-treated or germ-free rodents reveals alterations in
77 both stress responsiveness [19] and anxiety [20–22], although in germ-free models
78 these findings are complicated by the life-long absence of gut microbes and possible
79 consequent developmental alterations. Nonetheless, gut-microbe-depleted animals
80 have been shown to exhibit changes in serotonergic and glutamatergic neuronal
81 signalling [20] and expression of brain-derived neurotrophic factor (BDNF) within the
82 limbic system [22,23], providing a molecular correlate for behavioural changes.

83

84 Links between the gut microbiota and brain function have been identified in studies of
85 humans with autism spectrum disorders (ASD) and attention-deficit hyperactivity
86 disorder (ADHD). Altered microbial profiles have been identified in children with ASD
87 [24–26], and oral treatment of autistic children with the non-absorbed, broad-spectrum
88 antibiotic vancomycin – effectively suppressing the gut microbiota – led to a regression
89 in autistic behavioural characteristics that was reversed upon antibiotic discontinuation
90 [27]. Similarly, a small-scale intervention study has suggested not only a link between
91 lower counts of faecal *Bifidobacterium* species at six months and increased incidence
92 of ADHD at 13 years, but also that early probiotic treatment lessens the risk of ADHD
93 development [28].

94

95 A number of unresolved questions remain as to the mechanism(s) of communication
96 between the gut microbiota and the brain, but three major pathways have been
97 proposed: direct modification of vagal or sympathetic sensorimotor function [29],

98 inflammatory/immune activity [30] and neuroendocrine crosstalk [31]. While research
99 in this field has focussed most heavily on direct neural modulation and inflammatory
100 signalling, the potential role of circulating gut microbe-derived metabolites has been
101 relatively underexplored. Communication with and across the blood–brain barrier
102 (BBB), the primary interface between the circulation and the CNS, may therefore
103 represent a significant mechanism allowing the gut microbiota to influence brain
104 function.

105

106 There is accumulating evidence that the gut microbiota can affect the integrity of the
107 BBB, with both broad-spectrum-antibiotic-treated and germ-free mice exhibiting
108 considerably enhanced barrier permeability and dysregulation of inter-endothelial cell
109 tight junctions [32,33]. Importantly, these impairments can be reversed upon
110 conventionalisation. The mechanism(s) by which gut microbes exert their influence
111 are unclear, but changes to brain chemistry induced by alteration of the gut microbiota
112 can occur independently of vagal or sympathetic neural pathways and in the absence
113 of any immune response, strongly suggesting at least a contributory role for soluble
114 gut-derived microbial metabolites [22].

115

116 In particular, data highlight a potential role for short-chain fatty acids (SCFAs) as key
117 microbial mediators in the gut–brain axis. SCFAs are principally produced by the
118 fermentation of complex plant-based polysaccharides by gut bacteria and are potent
119 bioactive molecules; stimulating colonic blood flow and upper-gut motility, influencing
120 H₂O and NaCl uptake, providing energy for colonocytes, enhancing satiety and
121 positively influencing metabolic health in obese and diabetic individuals [34–36]. Of
122 the SCFAs, acetate is produced in the greatest quantity as a result of fermentation in

123 the large intestine, followed by propionate and butyrate [37]. Over 95 % of SCFAs
124 produced are absorbed within the colon with virtually none appearing in the urine or
125 faeces [35,38]. However, all three metabolites are detectable in the peripheral blood
126 of healthy individuals (<http://www.hmdb.ca>: acetate, 22–42 μM ; propionate, 0.9–1.2
127 μM ; butyrate, 0.3–1.5 μM). SCFAs activate members of the free fatty acid receptor
128 (FFAR) family of G protein coupled receptors; acetate, propionate and butyrate have
129 affinity in the low millimolar to high micromolar range for FFAR2; propionate and
130 butyrate have mid to low micromolar affinity for FFAR3 [39].

131

132 The majority of studies looking at the role of SCFAs in the gut–brain axis have focused
133 on butyrate [40], with relatively few investigating propionate despite its similar plasma
134 concentration and receptor affinity. Propionate is a highly potent FFAR3 agonist for its
135 size (agonist activity GTP γ S pEC₅₀ (E_{max}) 3.9-5.7(100%)) and has close to optimal
136 ligand efficiency ($-\Delta G=1.26 \text{ kcal mol}^{-1} \text{ atom}^{-1}$) for this receptor [41]. While propionate
137 has been shown to stimulate intestinal gluconeogenesis through direct stimulation of
138 enteric–CNS pathways [42], and increased intestinal propionate has been associated
139 with reduced stress behaviours [43] and reward pathway activity [44] in mice and
140 humans, respectively, its potential role as an endocrine mediator in the gut–brain axis
141 has not been addressed. Given the presence of FFAR3 on endothelial cells [45], we
142 hypothesised that propionate targeting of the endothelium of the BBB would represent
143 an additional facet of the gut–brain axis. We used a systems approach to test this
144 proposal, performing an unbiased study of the transcriptomic effects of exposure to
145 physiological levels of propionate upon the BBB, modelled by the immortalised human
146 cerebromicrovascular endothelial cell line hCMEC/D3, accompanied by *in vitro*
147 validation of identified pathway responses.

148

149 **Results**

150 *Microarray analyses*

151 Following initial confirmation of the expression of FFAR3 in human brain endothelium
152 (**Fig. 1a**) and on hCMEC/D3 cells (**Fig. 1b**), we investigated the effect of exposure of
153 hCMEC/D3 monolayers to 1 μ M propionate for 24 h. Such treatment had a significant
154 ($P_{\text{FDR}} < 0.1$) effect on the expression of 1136 genes: 553 upregulated, 583
155 downregulated (**Fig. 1c**). Initially, we used SPIA with all the significantly differentially
156 expressed genes to identify KEGG signalling pathways inhibited and activated in the
157 presence of propionate. Protein processing in the endoplasmic reticulum and RNA
158 transport were activated upon exposure of cells to propionate, which was unsurprising
159 given gene expression had been induced. A number of pathways associated with non-
160 specific microbial infections (Gram-negative bacteria, viral) were inhibited by
161 propionate (**Fig. 1d**), as were the cytosolic DNA-sensing pathway (upregulated by
162 pathogen DNA during microbial infections, triggering innate immune signalling [46]),
163 the NF κ B signalling pathway and the Toll-like receptor signalling pathway. Of the
164 19309 genes we examined on the array, 203 of the 224 genes known to be associated
165 with the BBB were detected (**Supplementary Table 1**). Eleven of these were
166 significantly differentially expressed, with the majority being associated with the
167 inflammatory response.

168

169 Enrichr [47,48] was used to examine KEGG pathways significantly associated with the
170 list of significantly differentially expressed genes. All 1136 significantly differentially
171 expressed genes mapped to Enrichr. As with SPIA, the genes were associated with

172 KEGG pathways implicated in non-specific microbial infections, and RNA- and
173 endoplasmic reticulum-associated processes (**Fig. 1e**).

174

175 WikiPathways analysis (Enrichr) of all the significantly differentially expressed genes
176 highlighted responses to oxidative stress being associated with propionate treatment
177 (not shown). Closer examination of the data demonstrated this was linked to NRF2
178 (NFE2L2) signaling, with the significantly upregulated genes closely associated with
179 oxidative stress responses (**Fig. 1f**).

180

181 *Pathway validation*

182 Transcriptomic analysis identified two particular clusters of pathways as being
183 regulated by propionate treatment: those involved in the non-specific inflammatory
184 response to microbial products (**Fig. 1d, e**) and those involved in the response to
185 oxidative stress (**Fig. 1f**). We, therefore, sought to validate these responses in an *in*
186 *vitro* model of the BBB.

187

188 *TLR-specific pathway*

189 Inhibition of the TLR-specific pathway by propionate suggests this metabolite may
190 have a protective role against exposure of the BBB to bacterial lipopolysaccharide
191 (LPS), derived from the cell walls of Gram-negative bacteria. In accord with this
192 hypothesis, exposure of hCMEC/D3 monolayers for 12 h to propionate at physiological
193 concentrations (1 μ M) was able to significantly attenuate the permeabilising effects of
194 exposure to *Escherichia coli* O111:B4 LPS (subsequent 12 h stimulation, 50 ng/ml),
195 measured both through paracellular permeability to a 70 kDa FITC-conjugated dextran
196 tracer (**Fig. 2a**) and trans-endothelial electrical resistance (**Fig. 2b**). To determine the

197 specificity of these effects for propionate, we investigated the actions of the closely
198 related SCFAs acetate and butyrate. While physiologically relevant circulating
199 concentrations of butyrate (1 μ M) replicated the effects of propionate on both trans-
200 endothelial electrical resistance and paracellular tracer permeability, this was not the
201 case for acetate (65 μ M) (**Fig. 2a-b**).

202

203 Circulating concentrations of propionate are approximately 1 μ M at rest, but these may
204 be expected to increase following consumption of, for example, a meal containing high
205 levels of fermentable fibre [1], consequently we examined the effects of 10 μ M and
206 100 μ M propionate upon the response of hCMEC/D3 monolayers to LPS stimulation.
207 Both LPS-induced deficits in trans-endothelial electrical resistance (**Suppl. Fig. 1a**)
208 and paracellular tracer permeability (**Suppl. Fig. 1b**) were fully attenuated by higher
209 doses of propionate, without any obvious further effects beyond those seen with 1 μ M
210 of the SCFA.

211

212 Although hCMEC/D3 cells are a widely used *in vitro* model of the BBB, they are not
213 without limitations, particularly in terms of their higher inherent permeability when
214 compared with other non-human model systems [49]. To ensure the validity of our
215 findings using hCMEC/D3 cells, we repeated these experiments using primary human
216 brain microvascular endothelial cells (HBMECs). As with hCMEC/D3 cells, exposure
217 of HBMEC monolayers for 12 h to propionate (1 μ M) significantly attenuated the
218 permeabilising effects of LPS exposure (subsequent 12 h stimulation, 50 ng/ml), in
219 terms of both paracellular permeability to a 70 kDa FITC-conjugated dextran tracer
220 (**Suppl Fig. 2a**) and trans-endothelial electrical resistance (**Suppl Fig. 2b**). Given this

221 confirmation, subsequent experiments focused solely on the hCMEC/D3 cells as an *in*
222 *vitro* BBB model.

223

224 Paracellular permeability and trans-endothelial electrical resistance are in large part
225 dependent upon the integrity of inter-endothelial tight junctions [50], which are known
226 to be disrupted following exposure to LPS [51]. We, therefore, examined the
227 intracellular distribution of the key tight junction components occludin, claudin-5 and
228 zona occludens-1 (ZO-1) following treatment with propionate and/or LPS. Exposure of
229 hCMEC/D3 monolayers to propionate alone (1 μ M, 24 h) had no noticeable effect on
230 the intracellular distribution of any of the studied tight junction components, whereas
231 treatment with LPS (50 ng/ml, 12 h) caused a marked disruption in the localisation of
232 all three major tight junction molecules, characterised by a loss of peri-membrane
233 immunoreactivity (**Fig. 2c**). Notably, these effects of LPS were substantially protected
234 against by prior treatment for 12 h with 1 μ M propionate.

235

236 LPS initiates a pro-inflammatory response through binding to Toll-like receptor 4,
237 TLR4, in a complex with the accessory proteins CD14 and LY96 (MD2) [52]; we,
238 therefore, examined expression of TLR4 signalling components as an explanation for
239 the protective effects of propionate upon this pathway. While propionate treatment of
240 hCMEC/D3 cells (1 μ M, 24 h) had no significant effect upon expression of mRNA for
241 TLR4 or LY96 (data not shown), such treatment significantly down-regulated
242 expression of *CD14* mRNA (**Fig. 2d**), an effect replicated at the level of cell surface
243 *CD14* protein expression (**Fig. 2e, f**).

244

245 *NFE2L2 (NRF2) signalling and protection from oxidative stress*

246 Enrichr (WikiPathways) analysis indicated that exposure of hCMEC/D3 cells to
247 propionate resulted in the regulation of a number of antioxidant systems. Of known
248 human anti-oxidant genes [53], 58 were detected on the array. We had also identified
249 an additional 6 genes via [54] (**Supplementary Table 2**). Searches of the genes
250 associated with each of the individual pathways referenced in **Fig. 1f** strongly indicated
251 these changes occurred downstream of the transcription factor nuclear factor,
252 erythroid 2 like 2 – NFE2L2 (**Fig. 3a**). Supporting this analysis, exposure of hCMEC/D3
253 cells for 24 h to 1 μ M propionate caused a marked translocation of NFE2L2 from the
254 cytoplasm to the nucleus (**Fig. 3b**). Functional analysis of antioxidant pathway activity
255 was assessed by monitoring reactive oxygen species production in hCMEC/D3 cells
256 following exposure to the mitochondrial complex I inhibitor rotenone (2.5 μ M, 2 h). Pre-
257 exposure of cells to 1 μ M propionate for 24 h significantly attenuated the rate of
258 fluorescent tracer accumulation, indicative of reduced levels of intracellular reactive
259 oxygen species (**Fig. 3c**).

260

261 *Efflux transporter expression and activity*

262 A key feature of the BBB is the expression of a wide array of efflux transporter proteins,
263 which limit entry of numerous endogenous and xenobiotic agents to, and promote their
264 export from, the brain. Amongst these, the proteins P-glycoprotein, BCRP and LRP-1
265 are prominent examples. We investigated the ability of propionate to both modify
266 expression of these transporters and, in the case of the ABC transporter proteins P-
267 glycoprotein and BCRP, serve as a direct inhibitor or substrate for the protein.
268 Exposure of hCMEC/D3 monolayers to propionate at physiological levels (1 μ M) for
269 24 h significantly suppressed expression of LRP-1 without modulating expression of
270 either BCRP or P-glycoprotein (**Supplementary Fig. 1a, b**). Similarly, propionate had

271 neither a stimulatory nor inhibitory effect upon either BCRP or P-glycoprotein activity,
272 at concentrations between 12 nM and 27 μ M (**Supplementary Fig. 1c-f**).

273

274 **Discussion**

275

276 Considerable effort has gone into interrogating the gut–brain axis over recent years,
277 with a steadily growing appreciation of the influence of the gut microbiota upon CNS
278 function in health and disease. Mechanistic studies have identified three principal
279 aspects to the gut–brain axis: modification of autonomic sensorimotor connections
280 [29], immune activation [30], and regulation of neuroendocrine pathways [31], all of
281 which incorporate a role for soluble gut-derived microbial agents, whether metabolic
282 products or structural microbial components (e.g. LPS) themselves. In the current
283 study, we identify a fourth facet to the gut–brain axis, namely the interactions between
284 gut-derived microbial metabolites and the primary defensive structure of the brain, the
285 BBB. In particular, we identify a beneficial, protective effect of the SCFA propionate
286 upon the BBB, mitigating against deleterious inflammatory and oxidative stimuli.

287

288 If confirmed *in vivo*, our findings of protective effects of propionate upon BBB
289 endothelial cells *in vitro* will add to the previously described beneficial actions of the
290 SCFA upon a number of metabolic parameters. Propionate has been shown to
291 improve glucose tolerance and insulin sensitivity, reduce high-density lipoprotein and
292 increase serum triglyceride concentrations [35,55,56], all of which result in a more
293 stable metabolic homeostasis. The effects of propionate upon the BBB that we
294 describe in this study add to these pro-homeostatic actions, emphasising the
295 contribution the SCFA plays to maintaining normal physiological function. Given that

296 the main source of circulating propionate in humans is the intestinal microbiota [57,58],
297 following fermentation of non-digestible carbohydrates by select bacterial species
298 (**Fig. 4**), propionate thus represents a paradigm of commensal, mutually beneficial
299 interactions between the host and microbiota. Moreover, consumption of food
300 containing non-digestible carbohydrates increases circulating propionate
301 concentrations approximately ten-fold [59,60], suggesting that the anti-inflammatory
302 effects of the SCFA upon the cerebrovascular endothelium may be another facet of
303 the known health benefits of high-fibre diets [61].

304

305 That BBB integrity is influenced by the gut microbiota and that SCFAs may play a role
306 in this process was recently emphasised in studies of germ-free vs. specific pathogen-
307 free mice, with germ-free animals exhibiting enhanced BBB permeability and disrupted
308 cerebral endothelial tight junctions [32]. These permeability defects were reversed fully
309 upon conventionalisation with a pathogen-free microbiota, and partially with
310 monocultures producing various SCFAs. Moreover, defective BBB integrity could be
311 ameliorated at least partially by extended oral administration of sodium butyrate. Our
312 findings thus cement SCFAs as a key group of gut-derived microbial mediators
313 modulating BBB function, and provide evidence emphasising a direct action through
314 the circulation. Propionate acts primarily through either of the two free fatty acid
315 receptors FFAR2 or FFAR3 [41], which although absent from neurones in the CNS
316 [62] have been identified in the cerebral endothelium [45], with FFAR3 confirmed
317 herein, indicating a possible mechanism of action. Although further study would be
318 required to prove it conclusively, our data suggest that FFAR3 may be the predominant
319 receptor type mediating the protective effects of SCFAs, as while the major ligands for
320 this receptor, propionate and butyrate, were both able to prevent a functional decline

321 in BBB integrity induced by LPS exposure, this was not the case for acetate, an SCFA
322 with greater potency at FFAR2 [39]. Future work investigating the relative contributions
323 of the two receptor types to BBB integrity will be informative.

324

325 Notably, and perhaps unsurprisingly, SCFAs cannot fully recapitulate the BBB-
326 restoring effects of conventionalisation of germ-free animals, as revealed in the current
327 work and previously [32,33]. It, therefore, seems likely that additional circulating gut-
328 derived microbial mediators may contribute to the regulation of BBB function, and are
329 thus highly deserving of future investigation. Given that upwards of 200 distinct
330 microbial metabolites have been identified in the circulation of healthy individuals and
331 animals [61,63], there is clearly great potential for intestinal dysbiosis and the resultant
332 variation in metabolite levels to influence the BBB.

333

334 This may be highly relevant to the development of neurological disease, as variation
335 in BBB function is increasingly recognised to impact on cognitive processes, although
336 the mechanism(s) underlying this link are poorly understood. In particular, defects in
337 BBB integrity have been linked with impaired memory [64] and linguistic [65] function,
338 as well as with inferior performance on psychometric tests such as the mini mental
339 state exam [66] and Oxford handicap scale [67]. Antibiotic-induced intestinal dysbiosis
340 has been associated with similar cognitive deficits and with a reduction in circulating
341 gut-derived microbial metabolites [33], but as yet whether the BBB plays a role in this
342 connection has not been investigated. If this is the case, however, as the current study
343 suggests, regulation of BBB function by microbe-derived mediators may be an
344 important component in some of the emerging links between intestinal dysbiosis and
345 pathologies as significant as depression [68], Parkinson's disease [69,70] and

346 Alzheimer's disease [71]. Notably, patients with early Parkinson's or Alzheimer's
347 diseases have been shown to bear reduced levels of *Bacteroides* species within their
348 faeces [71,72]. Given that *Bacteroides* spp. are important producers of SCFAs,
349 including propionate [57], from complex carbohydrates (**Fig. 4**), this reduction may
350 lead to a decline in circulating propionate and consequent vulnerability of the BBB,
351 and, by extension, the brain in these major neurological conditions.

352

353 Modulatory effects of circulating gut-derived microbial metabolites upon the BBB may
354 also be a component of the beneficial outcomes seen upon consumption of prebiotics
355 or probiotics in a number of neurological conditions. For example, small-scale clinical
356 trials have identified beneficial effects of probiotic drinks on cognitive ability in both
357 Alzheimer's disease [73] and multiple sclerosis [74], conditions associated with reduced
358 BBB integrity [75]. Similarly, oral administration of prebiotic oligosaccharides to mice
359 significantly reduced anxiety and stress behaviours, effects that correlated with
360 increases in caecal acetate, propionate and butyrate concentrations [43]. Whether such
361 changes in caecal SCFA reflected plasma levels was not measured, but given that
362 SCFAs can be transported across the gut epithelium [76,77] increases in circulating
363 concentrations may be likely. That inflammation contributes to depression has become
364 clearer over recent years [78], hence it is conceivable that the anti-inflammatory effects
365 of propionate we describe may underlie at least part of the protective effects of prebiotic
366 treatment, a proposal which, though speculative, is deserving of further study.

367

368 In summary, we reveal here a significant new aspect of the gut–brain axis, namely the
369 modulatory effects of circulating gut-derived microbial metabolites upon the
370 endothelium of the BBB. Given the critical gate-keeping role the BBB plays in

371 communication between the periphery and the brain parenchyma, our findings set the
372 stage for future investigation of the influence the gut microbiota has on this structure,
373 and the impact intestinal dysbiosis may have upon individual susceptibility to
374 neurological and psychological diseases.
375

376 **Materials & Methods**

377 *Human Tissue*

378 Human post mortem samples were taken from the prefrontal cortex from non-
379 neurologic controls; brains were retrieved from the UK Multiple Sclerosis Society
380 tissue bank at Imperial College London, under ethical approval from the UK MRC Brain
381 Bank Network (Ref. No. 08/MRE09/31+5). Brains were selected according to the
382 following criteria: (i) availability of full clinical history, (ii) no evidence of cancer post
383 mortem, and (iii) negligible atherosclerosis of cerebral vasculature. Tissue was fixed
384 in 10% v/v buffered formalin and embedded in paraffin. From each paraffin block, 5
385 μm sections were cut and used for immunohistochemistry for FFAR3 using standard
386 protocols [79], with a primary rabbit anti-FFAR3 polyclonal antibody (1:100; Stratech
387 Scientific, Newmarket, UK), a horseradish peroxidase-conjugated goat anti-rabbit
388 secondary antibody (1:300; Stratech Scientific, UK), and 2,3-diaminobenzidine and
389 hydrogen peroxide as chromogens. Images were taken using a Leica DM5000 bright-
390 field microscope equipped with a x40 oil immersion objective, and analysed using NIH
391 ImageJ 1.51h (National Institutes of Health, USA).

392

393 *Cerebromicrovascular cells*

394 The human cerebromicrovascular endothelial cell line hCMEC/D3 was purchased
395 from VHBio Ltd (Gateshead, UK), maintained and treated as described previously [79–
396 81]. Cells were cultured to confluency in complete EGM-2 endothelial cell growth
397 medium (Lonza, Basel, Switzerland), whereupon medium was replaced by EGM-2
398 without VEGF and cells were further cultured for a minimum of 4 days to enable
399 intercellular tight junction formation prior to experimentation. Primary human
400 cerebromicrovascular endothelial cells (HBMEC) were purchased from Sciencell

401 Research Laboratories (San Diego, CA, USA) and were maintained in ECM growth
402 medium according to the supplier's recommendations. Cells were cultured to
403 confluency in complete ECM (Sciencell Research Laboratories, USA), whereupon
404 medium was replaced by EGM-2 without VEGF and cells were further cultured for a
405 minimum of 4 days to enable intercellular tight junction formation prior to
406 experimentation. For primary cultures, trans-endothelial electrical resistance was
407 measured as described below, and experiments were only undertaken when this had
408 reached approximately 200 Ω .cm².

409

410 *Microarrays*

411 hCMEC/D3 cells were grown on 6-well plates coated with calf-skin collagen (Sigma-
412 Aldrich, Gillingham, UK) to confluency as described above, further cultured for 4 days
413 in EGM-2 medium without VEGF and exposed to propionate (1 μ M, 24 h). Cells were
414 collected into TRIzol (Thermo-Fisher Scientific, UK) and total RNA was extracted using
415 a TRIzol Plus RNA purification kit (Thermo-Fisher Scientific, UK) and quantified using
416 an ND-1000 Spectrophotometer (NanoDrop, Wilmington, USA).

417

418 Hybridization experiments were performed by MacroGen Inc. (Seoul, Korea) using
419 Illumina HumanHT-12 v4.0 Expression BeadChips (Illumina Inc., San Diego, CA).
420 RNA purity and integrity were evaluated using an ND-1000 Spectrophotometer
421 (NanoDrop, USA) and an Agilent 2100 Bioanalyzer (Agilent Technologies, Palo Alto,
422 USA). Total RNA was amplified and purified using TargetAmp-Nano Labelling Kit for
423 Illumina Expression BeadChip (EPICENTRE, Madison, USA) to yield biotinylated
424 cRNA according to the manufacturer's instructions. Briefly, 350 ng of total RNA was
425 reverse-transcribed to cDNA using a T7 oligo(dT) primer. Second-strand cDNA was

426 synthesized, *in vitro*-transcribed, and labelled with biotin-NTP. After purification, the
427 cDNA was quantified using the ND-1000 Spectrophotometer (NanoDrop, USA).

428

429 Labelled (750 ng) cDNA samples were hybridized to each beadchip for 17 h at 58 °C,
430 according to the manufacturer's instructions. Detection of array signal was carried out
431 using Amersham fluorolink streptavidin-Cy3 (GE Healthcare Bio-Sciences, Little
432 Chalfont, UK) following the bead array manual. Arrays were scanned with an Illumina
433 bead array reader confocal scanner according to the manufacturer's instructions. The
434 quality of hybridization and overall chip performance were monitored by visual
435 inspection of both internal quality control checks and the raw scanned data. Raw data
436 were extracted using the software provided by the manufacturer (Illumina
437 GenomeStudio v2011.1, Gene Expression Module v1.9.0).

438

439 *Processing and analyses of array data*

440 Raw data supplied by MacroGen were quality-checked, log₂-transformed and loess-
441 normalized (2 iterations) using affy [82]. Probes annotated as 'Bad' or 'No match' in
442 illuminaHumanv4.db [83] were removed from the dataset ($n = 13,631$) [84]. After this
443 filtering step, only probes with valid Entrez identifiers ($n = 28,979$) were retained for
444 further analyses. Entrez identifiers were matched to official gene symbols using
445 'Homo_sapiens.gene_info', downloaded from
446 <https://www.ncbi.nlm.nih.gov/guide/genes-expression/> on 14 January 2017. Average
447 gene expression values were used for identification of differentially expressed genes.
448 Array data have been deposited in ArrayExpress under accession number E-MTAB-
449 5686.

450

451 Signaling Pathway Impact Analysis (SPIA) was used to identify Kyoto Encyclopedia of
452 Genes and Genomes (KEGG) pathways activated or inhibited in hCMEC/D3 cells
453 exposed to propionate [85]. Enrichr [47,48] was used to confirm KEGG findings (with
454 respect to pathways, not their activation/inhibition) and to perform Gene Ontology
455 (GO)- and WikiPathways-based analyses.

456

457 *In vitro barrier function assessments*

458 Paracellular permeability and transendothelial electrical resistance were measured on
459 100 % confluent cultures polarised by growth on 24-well plate polyethylene
460 terephthalate (PET) transwell inserts (surface area: 0.33 cm², pore size: 0.4 μm;
461 Appleton Woods, UK) coated with calf-skin collagen and fibronectin (Sigma-Aldrich,
462 UK). The permeability of endothelial cell monolayers to 70 kDa FITC-dextran (2 mg/ml)
463 was measured as described previously [81,86,87]; data are presented as the
464 contribution to the permeability barrier provided by endothelial cells, P_e, throughout.
465 Transendothelial electrical resistance (TEER) measurements were performed using a
466 Millicell ERS-2 Voltohmmeter (Millipore, Watford, UK) and were expressed as Ω.cm².
467 In all cases, values obtained from cell-free inserts similarly coated with collagen and
468 fibronectin were subtracted from the total values. Briefly, cells were treated with
469 propionate (1 μM) for 24 h prior to analysis of barrier function. In some cases, barrier
470 integrity was tested by challenge with bacterial lipopolysaccharide (LPS). Confluent
471 endothelial monolayers were treated with propionate (1 μM) for 12 h, whereupon LPS
472 (*Escherichia coli* O111:B4; 50 ng/ml, comparable to circulating levels of LPS in human
473 endotoxemia [88]) was added for a further 12 h, without wash-out. Barrier function
474 characteristics were then interrogated as described above.

475

476 *Efflux transporter assays*

477 Activity of the major efflux transporters P-glycoprotein and BCRP [89] was determined
478 through the use of commercially available assays (Solvo Biotechnology Inc.,
479 Budapest, Hungary), performed according to the manufacturer's instructions. Step-
480 wise dose-response curves centred around reported physiological circulating
481 concentrations of propionate [90] were constructed (n=2) and both activating and
482 inhibitory effects of propionate upon transporter activity were analysed.

483

484 *Flow cytometry analysis*

485 hCMEC/D3 cells were labelled with APC-conjugated mouse monoclonal anti-CD14
486 (Thermo-Fisher Scientific, Paisley, UK), APC-conjugated mouse monoclonal anti-
487 BCRP (BD Biosciences, Oxford, UK), FITC-conjugated mouse monoclonal LRP1 (BD
488 Biosciences, UK), PE-conjugated mouse monoclonal anti-MDR1A (BD Biosciences,
489 UK), unconjugated rabbit polyclonal antibody directed against FFAR3/GPR41
490 (Flarebio Biotech LLC, College Park, MD, USA) followed by incubation with an AF488-
491 conjugated goat anti-rabbit secondary antibody (Thermo-Fisher Scientific, UK), or
492 appropriate isotype controls (all BD Biosciences, UK) for analysis by flow cytometry.
493 Briefly, hCMEC/D3 cells were treated for 24 h with propionate (1 μ M), detached using
494 0.05 % trypsin and incubated with antibodies as described above.
495 Immunofluorescence was analysed for 20,000 events per treatment using a BD
496 FACSCanto II (BD Biosciences, UK) flow cytometer and data were analysed using
497 FlowJo 8.0 software (Treestar Inc., CA, USA).

498

499 *Immunofluorescence analysis*

500 hCMEC/D3 cells were cultured on Lab-Tek™ Permax™ 8-well chamber slides
501 coated with calf-skin collagen (Sigma-Aldrich, UK), prior to immunostaining according
502 to standard protocols [79,81] and using primary antibodies directed against Nrf2
503 (1:500, Novus Biologicals Ltd., Abingdon, UK), occludin (1:200, Thermo-Fisher
504 Scientific, UK), claudin-5 (1:200, Thermo-Fisher Scientific, UK) and zona occludens-1
505 (ZO-1; 1:100, Thermo-Fisher Scientific, UK). Nuclei were counterstained with DAPI
506 (Sigma-Aldrich, UK). Images were captured using an LSM880 confocal laser scanning
507 microscope (Carl Zeiss Ltd., Cambridge, UK) fitted with 405 nm, 488 nm, and 561 nm
508 lasers, and a 63x oil immersion objective lens (NA, 1.4 mm, working distance, 0.17
509 mm). Images were captured with ZEN imaging software (Carl Zeiss Ltd., UK) and
510 analysed using ImageJ 1.51h (National Institutes of Health, USA).

511

512 *Statistical analyses*

513 Sample sizes were calculated to detect differences of 15 % or more with a power of
514 0.85 and α set at 5 %, calculations being informed by previously published data
515 [79,81]. *In vitro* experimental data are expressed as mean \pm SEM, with $n=3$
516 independent experiments performed in triplicate for all studies. In all cases, normality
517 of distribution was established using the Shapiro–Wilkes test, followed by analysis with
518 two-tailed Student's *t*-tests to compare two groups or, for multiple comparison
519 analysis, 1- or 2-way ANOVA followed by Tukey's HSD *post hoc* test. Where data was
520 not normally distributed, non-parametric analysis was performed using the Wilcoxon
521 signed rank test. A *P* value of less than or equal to 5 % was considered significant.
522 Differentially expressed genes were identified in microarray data using LIMMA [91]; *P*
523 values were corrected for multiple testing using the Benjamini–Hochberg procedure

524 (False Discovery Rate); a P value of less than or equal to 10 % was considered
525 significant in this case.

526

527 **Declarations**

528

529 *Ethics approval and consent to participate*

530 Not applicable

531

532 *Consent for publication*

533 Not applicable

534

535 *Availability of data and material*

536 Array data have been deposited in ArrayExpress under accession number E-MTAB-
537 5686 (<http://www.ebi.ac.uk/arrayexpress/experiments/E-MTAB-5686/>)

538

539 *Competing interests*

540 The authors declare that they have no competing interests

541

542 *Funding*

543 This work was funded by Alzheimer's Research UK Pilot Grant no. ARUK-PPG2016B-
544 6. This work used the computing resources of the UK MEDical BIOinformatics
545 partnership – aggregation, integration, visualization and analysis of large, complex
546 data (UK MED-BIO), which is supported by the Medical Research Council (grant
547 number MR/L01632X/1). Human tissue samples and associated clinical and
548 neuropathological data were supplied by the Multiple Sclerosis Society Tissue Bank,

549 funded by the Multiple Sclerosis Society of Great Britain and Northern Ireland,
550 registered charity 207495. LH is in receipt of an MRC Intermediate Research
551 Fellowship in Data Science (MR/L01632X/1, UK MED-BIO). TS received a bursary
552 from Imperial College London as part of the Undergraduate Research Opportunities
553 Programme.

554

555 *Authors' contributions*

556 LH and SM conceived the experiments; LH, TS, UU and SM performed experiments;
557 LH and SM analysed the data; LH and SM wrote the paper; JKN, SRC and RCG
558 provided valuable insight and advice throughout the project.

559

560 *Acknowledgements*

561 Not applicable

562

563 **References**

564

565 1. Nicholson JK, Holmes E, Kinross J, Burcelin R, Gibson G, Jia W, et al. Host-gut
566 microbiota metabolic interactions. *Science*. 2012;336:1262–7.

567 2. Forslund K, Hildebrand F, Nielsen T, Falony G, Le Chatelier E, Sunagawa S, et al.
568 Disentangling type 2 diabetes and metformin treatment signatures in the human gut
569 microbiota. *Nature*. 2015;528:262–6.

570 3. Ley RE, Bäckhed F, Turnbaugh P, Lozupone CA, Knight RD, Gordon JI. Obesity
571 alters gut microbial ecology. *Proc. Natl. Acad. Sci. U. S. A.* 2005;102:11070–5.

- 572 4. Manichanh C, Rigottier-Gois L, Bonnaud E, Gloux K, Pelletier E, Frangeul L, et al.
573 Reduced diversity of faecal microbiota in Crohn's disease revealed by a metagenomic
574 approach. *Gut*. 2006;55:205–11.
- 575 5. Turnbaugh PJ, Hamady M, Yatsunencko T, Cantarel BL, Duncan A, Ley RE, et al. A
576 core gut microbiome in obese and lean twins. *Nature*. 2009;457:480–4.
- 577 6. Qin N, Yang F, Li A, Prifti E, Chen Y, Shao L, et al. Alterations of the human gut
578 microbiome in liver cirrhosis. *Nature*. 2014;513:59–64.
- 579 7. Monaco CL, Gootenberg DB, Zhao G, Handley SA, Ghebremichael MS, Lim ES, et
580 al. Altered Virome and Bacterial Microbiome in Human Immunodeficiency Virus-
581 Associated Acquired Immunodeficiency Syndrome. *Cell Host Microbe*. 2016;19:311–
582 22.
- 583 8. Smith MI, Yatsunencko T, Manary MJ, Trehan I, Mkakosya R, Cheng J, et al. Gut
584 microbiomes of Malawian twin pairs discordant for kwashiorkor. *Science*.
585 2013;339:548–54.
- 586 9. Campbell SC, Wisniewski PJ, Noji M, McGuinness LR, Häggblom MM, Lightfoot
587 SA, et al. The Effect of Diet and Exercise on Intestinal Integrity and Microbial Diversity
588 in Mice. *PLoS One*. 2016;11:e0150502.
- 589 10. Shoaie S, Ghaffari P, Kovatcheva-Datchary P, Mardinoglu A, Sen P, Pujos-Guillot
590 E, et al. Quantifying Diet-Induced Metabolic Changes of the Human Gut Microbiome.
591 *Cell Metab*. 2015;22:320–31.
- 592 11. Zhu B, Wang X, Li L. Human gut microbiome: the second genome of human body.
593 *Protein Cell*. 2010;1:718–25.
- 594 12. Patterson E, Cryan JF, Fitzgerald GF, Ross RP, Dinan TG, Stanton C. Gut
595 microbiota, the pharmabiotics they produce and host health. *Proc. Nutr. Soc.*
596 2014;73:477–89.
- 597 13. Li M, Wang B, Zhang M, Rantalainen M, Wang S, Zhou H, et al. Symbiotic gut
598 microbes modulate human metabolic phenotypes. *Proc. Natl. Acad. Sci.*
599 2008;105:2117–22.

- 600 14. Zheng X, Zhao A, Xie G, Chi YY, Zhao L, Li H, et al. Melamine-induced renal
601 toxicity is mediated by the gut microbiota. *Sci. Transl. Med.* 2013;5:172ra22.
- 602 15. Kindinger LM, MacIntyre DA, Lee YS, Marchesi JR, Smith A, McDonald JAK, et al.
603 Relationship between vaginal microbial dysbiosis, inflammation, and pregnancy
604 outcomes in cervical cerclage. *Sci. Transl. Med.* 2016;8:350ra102.
- 605 16. Bhat MI, Kapila R. Dietary metabolites derived from gut microbiota: critical
606 modulators of epigenetic changes in mammals. *Nutr. Rev.* 2017;75:374–89.
- 607 17. Krautkramer KA, Rey FE, Denu JD. Chemical signaling between gut microbiota
608 and host chromatin: What is your gut really saying? *J. Biol. Chem.*
609 2017;jbc.R116.761577.
- 610 18. Sherwin E, Rea K, Dinan TG, Cryan JF. A gut (microbiome) feeling about the brain.
611 *Curr. Opin. Gastroenterol.* 2016;32:96–102.
- 612 19. Sudo N, Chida Y, Aiba Y, Sonoda J, Oyama N, Yu X-N, et al. Postnatal microbial
613 colonization programs the hypothalamic-pituitary-adrenal system for stress response
614 in mice. *J. Physiol.* 2004;558:263–75.
- 615 20. Neufeld KM, Kang N, Bienenstock J, Foster JA. Reduced anxiety-like behavior
616 and central neurochemical change in germ-free mice. *Neurogastroenterol. Motil.*
617 2011;23:255–e119.
- 618 21. Heijtz RD, Wang S, Anuar F, Qian Y, Bjorkholm B, Samuelsson A, et al. Normal
619 gut microbiota modulates brain development and behavior. *Proc. Natl. Acad. Sci.*
620 2011;108:3047–52.
- 621 22. Bercik P, Denou E, Collins J, Jackson W, Lu J, Jury J, et al. The intestinal
622 microbiota affect central levels of brain-derived neurotropic factor and behavior in
623 mice. *Gastroenterology.* 2011;141:599–609, 609.e1–3.
- 624 23. Hoban AE, Moloney RD, Golubeva AV, McVey Neufeld KA, O’Sullivan O,
625 Patterson E, et al. Behavioural and neurochemical consequences of chronic gut
626 microbiota depletion during adulthood in the rat. *Neuroscience.* 2016;339:463–77.

- 627 24. Finegold SM, Downes J, Summanen PH. Microbiology of regressive autism.
628 *Anaerobe*. 2012;18:260–2.
- 629 25. Finegold SM, Dowd SE, Gontcharova V, Liu C, Henley KE, Wolcott RD, et al.
630 Pyrosequencing study of fecal microflora of autistic and control children. *Anaerobe*.
631 2010;16:444–53.
- 632 26. Mezzelani A, Landini M, Facchiano F, Raggi ME, Villa L, Molteni M, et al.
633 Environment, dysbiosis, immunity and sex-specific susceptibility: A translational
634 hypothesis for regressive autism pathogenesis. *Nutr. Neurosci*. 2015;18:145–61.
- 635 27. Sandler RH, Finegold SM, Bolte ER, Buchanan CP, Maxwell AP, Vaisanen M-L,
636 et al. Short-Term Benefit From Oral Vancomycin Treatment of Regressive-Onset
637 Autism. *J. Child Neurol*. 2000;15:429–35.
- 638 28. Pärtty A, Kalliomäki M, Wacklin P, Salminen S, Isolauri E. A possible link between
639 early probiotic intervention and the risk of neuropsychiatric disorders later in childhood:
640 a randomized trial. *Pediatr. Res*. 2015;77:823–8.
- 641 29. Forsythe P, Bienenstock J, Kunze WA. Vagal pathways for microbiome-brain-gut
642 axis communication. *Adv. Exp. Med. Biol*. 2014;817:115–33.
- 643 30. Powell N, Walker MM, Talley NJ. The mucosal immune system: master regulator
644 of bidirectional gut–brain communications. *Nat. Rev. Gastroenterol. Hepatol*.
645 2017;14:143–59.
- 646 31. Cani PD, Knauf C. How gut microbes talk to organs: The role of endocrine and
647 nervous routes. *Mol. Metab. Elsevier*; 2016;5:743–52.
- 648 32. Braniste V, Al-Asmakh M, Kowal C, Anuar F, Abbaspour A, Tóth M, et al. The gut
649 microbiota influences blood-brain barrier permeability in mice. *Sci. Transl. Med*.
650 2014;6:263ra158.
- 651 33. Fröhlich EE, Farzi A, Mayerhofer R, Reichmann F, Jačan A, Wagner B, et al.
652 Cognitive Impairment by Antibiotic-Induced Gut Dysbiosis: Analysis of Gut Microbiota-
653 Brain Communication. *Brain. Behav. Immun*. 2016;56:140–55.

- 654 34. Roediger WE. Role of anaerobic bacteria in the metabolic welfare of the colonic
655 mucosa in man. *Gut*. 1980;21:793–8.
- 656 35. Salminen S, Bouley C, Boutron-Ruault MC, Cummings JH, Franck A, Gibson GR,
657 et al. Functional food science and gastrointestinal physiology and function. *Br. J. Nutr.*
658 1998;80 Suppl 1:S147–71.
- 659 36. Frost G, Sleeth ML, Sahuri-Arisoylu M, Lizarbe B, Cerdan S, Brody L, et al. The
660 short-chain fatty acid acetate reduces appetite via a central homeostatic mechanism.
661 *Nat. Commun. Nature Publishing Group*; 2014;5:672–9.
- 662 37. Cummings JH, Pomare EW, Branch WJ, Naylor CP, Macfarlane GT. Short chain
663 fatty acids in human large intestine, portal, hepatic and venous blood. *Gut*.
664 1987;28:1221–7.
- 665 38. Topping DL, Clifton PM. Short-chain fatty acids and human colonic function: roles
666 of resistant starch and nonstarch polysaccharides. *Physiol. Rev.* 2001;81:1031–64.
- 667 39. Alexander SP, Davenport AP, Kelly E, Marrion N, Peters JA, Benson HE, et al.
668 The Concise Guide to PHARMACOLOGY 2015/16: G protein-coupled receptors. *Br.*
669 *J. Pharmacol.* 2015;172:5744–869.
- 670 40. Stilling RM, van de Wouw M, Clarke G, Stanton C, Dinan TG, Cryan JF. The
671 neuropharmacology of butyrate: The bread and butter of the microbiota-gut-brain axis?
672 *Neurochem. Int.* 2016;99:110–32.
- 673 41. Schmidt J, Smith NJ, Christiansen E, Tikhonova IG, Grundmann M, Hudson BD,
674 et al. Selective orthosteric free fatty acid receptor 2 (FFA2) agonists: identification of
675 the structural and chemical requirements for selective activation of FFA2 versus FFA3.
676 *J. Biol. Chem.* 2011;286:10628–40.
- 677 42. De Vadder F, Kovatcheva-Datchary P, Goncalves D, Vinera J, Zitoun C, Duchamp
678 A, et al. Microbiota-generated metabolites promote metabolic benefits via gut-brain
679 neural circuits. *Cell*. 2014;156:84–96.
- 680 43. Burokas A, Arboleya S, Moloney RD, Peterson VL, Murphy K, Clarke G, et al.
681 Targeting the Microbiota-Gut-Brain Axis: Prebiotics Have Anxiolytic and

682 Antidepressant-like Effects and Reverse the Impact of Chronic Stress in Mice. *Biol.*
683 *Psychiatry.* 2017;82:472–87.

684 44. Byrne CS, Chambers ES, Alhabeeb H, Chhina N, Morrison DJ, Preston T, et al.
685 Increased colonic propionate reduces anticipatory reward responses in the human
686 striatum to high-energy foods. *Am. J. Clin. Nutr.* 2016;104:5–14.

687 45. Brown AJ, Goldsworthy SM, Barnes AA, Eilert MM, Tcheang L, Daniels D, et al.
688 The Orphan G protein-coupled receptors GPR41 and GPR43 are activated by
689 propionate and other short chain carboxylic acids. *J. Biol. Chem. American Society for*
690 *Biochemistry and Molecular Biology;* 2003;278:11312–9.

691 46. Radoshevich L, Dussurget O. Cytosolic Innate Immune Sensing and Signaling
692 upon Infection. *Front. Microbiol.* 2016;7:313.

693 47. Chen EY, Tan CM, Kou Y, Duan Q, Wang Z, Meirelles GV, et al. Enrichr: interactive
694 and collaborative HTML5 gene list enrichment analysis tool. *BMC Bioinformatics.*
695 2013;14:128.

696 48. Kuleshov M V, Jones MR, Rouillard AD, Fernandez NF, Duan Q, Wang Z, et al.
697 Enrichr: a comprehensive gene set enrichment analysis web server 2016 update.
698 *Nucleic Acids Res.* 2016;44:W90–7.

699 49. Helms HC, Abbott NJ, Burek M, Cecchelli R, Couraud P-O, Deli MA, et al. In vitro
700 models of the blood-brain barrier: An overview of commonly used brain endothelial
701 cell culture models and guidelines for their use. *J. Cereb. Blood Flow Metab.*
702 2016;36:862–90.

703 50. Haseloff RF, Dithmer S, Winkler L, Wolburg H, Blasig IE. Transmembrane proteins
704 of the tight junctions at the blood-brain barrier: structural and functional aspects.
705 *Semin. Cell Dev. Biol.* 2015;38:16–25.

706 51. Varatharaj A, Galea I. The blood-brain barrier in systemic inflammation. *Brain.*
707 *Behav. Immun.* 2016;60:1–12.

708 52. Peri F, Piazza M, Calabrese V, Damore G, Cighetti R. Exploring the LPS/TLR4
709 signal pathway with small molecules. *Biochem. Soc. Trans.* 2010;38:1390–5.

- 710 53. Gelain DP, Dalmolin RJS, Belau VL, Moreira JCF, Klamt F, Castro MAA. A
711 systematic review of human antioxidant genes. *Front. Biosci. (Landmark Ed.*
712 *2009;14:4457–63.*
- 713 54. Gorrini C, Harris IS, Mak TW. Modulation of oxidative stress as an anticancer
714 strategy. *Nat. Rev. Drug Discov.* 2013;12:931–47.
- 715 55. Todesco T, Rao A V, Bosello O, Jenkins DJ. Propionate lowers blood glucose and
716 alters lipid metabolism in healthy subjects. *Am. J. Clin. Nutr.* 1991;54:860–5.
- 717 56. Venter CS, Vorster HH, Cummings JH. Effects of dietary propionate on
718 carbohydrate and lipid metabolism in healthy volunteers. *Am. J. Gastroenterol.*
719 *1990;85:549–53.*
- 720 57. Reichardt N, Duncan SH, Young P, Belenguer A, McWilliam Leitch C, Scott KP, et
721 al. Phylogenetic distribution of three pathways for propionate production within the
722 human gut microbiota. *ISME J.* 2014;8:1323–35.
- 723 58. Vogt JA, Wolever TMS. Fecal acetate is inversely related to acetate absorption
724 from the human rectum and distal colon. *J. Nutr.* 2003;133:3145–8.
- 725 59. Vogt JA, Pencharz PB, Wolever TMS. L-Rhamnose increases serum propionate
726 in humans. *Am. J. Clin. Nutr.* 2004;80:89–94.
- 727 60. Nilsson AC, Östman EM, Knudsen KEB, Holst JJ, Björck IME. A Cereal-Based
728 Evening Meal Rich in Indigestible Carbohydrates Increases Plasma Butyrate the Next
729 Morning^{1,2}. *J. Nutr.* 2010;140:1932–6.
- 730 61. Russell WR, Hoyles L, Flint HJ, Dumas M-E. Colonic bacterial metabolites and
731 human health. *Curr. Opin. Microbiol.* 2013;16:246–54.
- 732 62. Nohr MK, Egerod KL, Christiansen SH, Gille A, Offermanns S, Schwartz TW, et
733 al. Expression of the short chain fatty acid receptor GPR41/FFAR3 in autonomic and
734 somatic sensory ganglia. *Neuroscience.* 2015;290:126–37.
- 735 63. Zheng X, Xie G, Zhao A, Zhao L, Yao C, Chiu NHL, et al. The footprints of gut
736 microbial-mammalian co-metabolism. *J. Proteome Res.* 2011;10:5512–22.

- 737 64. Montagne A, Barnes SR, Sweeney MD, Halliday MR, Sagare AP, Zhao Z, et al.
738 Blood-Brain Barrier Breakdown in the Aging Human Hippocampus. *Neuron*.
739 2015;85:296–302.
- 740 65. Taheri S, Gasparovic C, Huisa BN, Adair JC, Edmonds E, Prestopnik J, et al.
741 Blood-brain barrier permeability abnormalities in vascular cognitive impairment.
742 *Stroke*. 2011;42:2158–63.
- 743 66. Bowman GL, Kaye JA, Moore M, Waichunas D, Carlson NE, Quinn JF. Blood-
744 brain barrier impairment in Alzheimer disease: stability and functional significance.
745 *Neurology*. 2007;68:1809–14.
- 746 67. Wardlaw JM, Doubal FN, Valdes-Hernandez M, Wang X, Chappell FM, Shuler K,
747 et al. Blood-brain barrier permeability and long-term clinical and imaging outcomes in
748 cerebral small vessel disease. *Stroke*. 2013;44:525–7.
- 749 68. Aizawa E, Tsuji H, Asahara T, Takahashi T, Teraishi T, Yoshida S, et al. Possible
750 association of Bifidobacterium and Lactobacillus in the gut microbiota of patients with
751 major depressive disorder. *J. Affect. Disord*. 2016;202:254–7.
- 752 69. Scheperjans F, Aho V, Pereira PAB, Koskinen K, Paulin L, Pekkonen E, et al. Gut
753 microbiota are related to Parkinson’s disease and clinical phenotype. *Mov. Disord*.
754 2015;30:350–8.
- 755 70. Petrov VA, Saltykova I V, Zhukova IA, Alifirova VM, Zhukova NG, Dorofeeva YB,
756 et al. Analysis of Gut Microbiota in Patients with Parkinson’s Disease. *Bull. Exp. Biol*.
757 *Med*. 2017;162:734–7.
- 758 71. Cattaneo A, Cattane N, Galluzzi S, Provasi S, Lopizzo N, Festari C, et al.
759 Association of brain amyloidosis with pro-inflammatory gut bacterial taxa and
760 peripheral inflammation markers in cognitively impaired elderly. *Neurobiol. Aging*.
761 2017;49:60–8.
- 762 72. Bedarf JR, Hildebrand F, Coelho LP, Sunagawa S, Bahram M, Goeser F, et al.
763 Functional implications of microbial and viral gut metagenome changes in early stage
764 L-DOPA-naive Parkinson’s disease patients. *Genome Med*. 2017;9:39.

- 765 73. Akbari E, Asemi Z, Daneshvar Kakhaki R, Bahmani F, Kouchaki E, Tamtaji OR, et
766 al. Effect of Probiotic Supplementation on Cognitive Function and Metabolic Status in
767 Alzheimer's Disease: A Randomized, Double-Blind and Controlled Trial. *Front. Aging*
768 *Neurosci.* 2016;8:256.
- 769 74. Kouchaki E, Tamtaji OR, Salami M, Bahmani F, Daneshvar Kakhaki R, Akbari E,
770 et al. Clinical and metabolic response to probiotic supplementation in patients with
771 multiple sclerosis: A randomized, double-blind, placebo-controlled trial. *Clin. Nutr.*
772 2016;36:1245–9.
- 773 75. Engelhardt B, Sorokin L. The blood-brain and the blood-cerebrospinal fluid
774 barriers: function and dysfunction. *Semin. Immunopathol.* 2009;31:497–511.
- 775 76. Gonçalves P, Araújo JR, Pinho MJ, Martel F. Modulation of butyrate transport in
776 Caco-2 cells. *Naunyn. Schmiedebergs. Arch. Pharmacol.* 2009;379:325–36.
- 777 77. Stein J, Zores M, Schröder O. Short-chain fatty acid (SCFA) uptake into Caco-2
778 cells by a pH-dependent and carrier mediated transport mechanism. *Eur. J. Nutr.*
779 2000;39:121–5.
- 780 78. Pariante CM. Why are depressed patients inflamed? A reflection on 20 years of
781 research on depression, glucocorticoid resistance and inflammation. *Eur.*
782 *Neuropsychopharmacol.* 2017;27:554–9.
- 783 79. Cristante E, McArthur S, Mauro C, Maggioli E, Romero IAIA, Wylezinska-Arridge
784 M, et al. Identification of an essential endogenous regulator of blood-brain barrier
785 integrity, and its pathological and therapeutic implications. *Proc. Natl. Acad. Sci. U. S.*
786 *A.* 2013/01/02 ed. 2013;110:832–41.
- 787 80. Weksler BB, Subileau EA, Perrière N, Charneau P, Holloway K, Leveque M, et al.
788 Blood-brain barrier-specific properties of a human adult brain endothelial cell line.
789 *FASEB J.* 2005;19:1872–4.
- 790 81. Maggioli E, McArthur S, Mauro C, Kieswich J, Kusters DHM, Reutelingsperger
791 CPMPM, et al. Estrogen protects the blood-brain barrier from inflammation-induced
792 disruption and increased lymphocyte trafficking. *BRAIN, Behav. Immun.* 2015;51:212–
793 22.

- 794 82. Gautier L, Cope L, Bolstad BM, Irizarry RA. affy--analysis of Affymetrix GeneChip
795 data at the probe level. *Bioinformatics*. 2004;20:307–15.
- 796 83. Dunning M, Lynch A, Eldridge M. illuminaHumanv4.db: Illumina HumanHT12v4
797 annotation data (chip illuminaHumanv4). 2015.
- 798 84. Ritchie ME, Dunning MJ, Smith ML, Shi W, Lynch AG. BeadArray expression
799 analysis using bioconductor. Lewitter F, editor. *PLoS Comput. Biol.* 2011;7:e1002276.
- 800 85. Tarca AL, Draghici S, Khatri P, Hassan SS, Mittal P, Kim J-S, et al. A novel
801 signaling pathway impact analysis. *Bioinformatics*. 2009;25:75–82.
- 802 86. Abbott NJ, Hughes CC, Revest PA, Greenwood J. Development and
803 characterisation of a rat brain capillary endothelial culture: towards an in vitro blood-
804 brain barrier. *J. Cell Sci.* 1992;103 (Pt 1:23–37.
- 805 87. Coisne C, Dehouck L, Faveeuw C, Delplace Y, Miller F, Landry C, et al. Mouse
806 syngenic in vitro blood-brain barrier model: a new tool to examine inflammatory events
807 in cerebral endothelium. *Lab. Invest.* 2005;85:734–46.
- 808 88. Pais de Barros J-P, Gautier T, Sali W, Adrie C, Choubley H, Charron E, et al.
809 Quantitative lipopolysaccharide analysis using HPLC/MS/MS and its combination with
810 the limulus amoebocyte lysate assay. *J. Lipid Res. American Society for Biochemistry
811 and Molecular Biology*; 2015;56:1363–9.
- 812 89. Löscher W, Potschka H. Blood-brain barrier active efflux transporters: ATP-binding
813 cassette gene family. *NeuroRx. Am. Soc. for Experimental NeuroTherapeutics*;
814 2005;2:86–98.
- 815 90. Wishart DS, Jewison T, Guo AC, Wilson M, Knox C, Liu Y, et al. HMDB 3.0--The
816 Human Metabolome Database in 2013. *Nucleic Acids Res.* 2013;41:D801–7.
- 817 91. Ritchie ME, Phipson B, Wu D, Hu Y, Law CW, Shi W, et al. limma powers
818 differential expression analyses for RNA-sequencing and microarray studies. *Nucleic
819 Acids Res.* 2015;43:e47.

820

821 **Figure Legends**

822

823 **Fig. 1:** Effects on gene expression of exposure of the hCMEC/D3 cell line to
824 propionate (1 μ M, 24 h). (a) Representative images of FFAR3 immunoreactivity within
825 endothelial cells of capillaries (i) and larger post-capillary (ii) blood vessels in control
826 human brains *post mortem*; scale bar 20 μ m, sections are 5 μ m thick; images are
827 representative of five independent cases, areas of particular immunoreactivity are
828 highlighted by black arrowheads. (b) Surface expression of FFAR3/GPR41 by
829 hCMEC/D3 cells (grey line, unstained cells, black line secondary antibody control, red
830 line FFAR3), data are representative of three independent experiments. (c) Volcano
831 plot showing significantly ($P_{\text{FDR}} < 0.1$, red dots) differentially expressed genes. The top
832 20 up- and down-regulated genes are labelled. (d) SPIA evidence plot for the 1136
833 significantly differentially expressed genes. Only those human KEGG pathways
834 associated with non-specific microbial infections are labelled. The pathways at the
835 right of the red oblique line are significant ($P < 0.2$) after Bonferroni correction of the
836 global P values, pG, obtained by combining the pPERT and pNDE using the normal
837 inversion method. The pathways at the right of the blue oblique line are significant (P
838 < 0.2) after a FDR correction of the global P values, pG. 04810, Regulation of actin
839 cytoskeleton (inhibited); 04064, NF-kappa B signaling pathway (inhibited); 04978,
840 Mineral absorption (inhibited); 03013, RNA transport (activated); 04141, Protein
841 processing in endoplasmic reticulum (activated); 04350, TGF-beta signaling pathway
842 (activated); 04623, Cytosolic DNA-sensing pathway (inhibited). (e) Association of all
843 significantly differentially expressed genes ($n = 1136$) with KEGG pathways, Enrichr.
844 (f) Association of all significantly upregulated genes ($n = 553$) with WikiPathways,
845 Enrichr. (e, f) The lighter in colour and the longer the bars, the more significant the

846 result is. Significance of data was determined using rank-based ranking; only the top
847 10 results are shown in each case.

848

849 **Fig. 2:** Protective effects of propionate against LPS-induced barrier disruption. (a)
850 Assessment of the paracellular permeability of hCMEC/D3 monolayers to 70 kDa
851 FITC-dextran following treatment for 24 h with 65 μ M acetate, 1 μ M butyrate or 1 μ M
852 propionate, with or without inclusion of 50 ng/ml LPS for the last 12 h of incubation;
853 data are mean \pm SEM, $n = 3$ independent experiments. (b) Trans-endothelial electrical
854 resistance of hCMEC/D3 monolayers following treatment for 24 h with 65 μ M acetate,
855 1 μ M butyrate or 1 μ M propionate, with or without inclusion of 50 ng/ml LPS for the
856 last 12 h of incubation; data are mean \pm SEM, $n = 3$ independent experiments. (c)
857 Confocal microscopic analysis of expression of the tight junction components claudin-
858 5, occludin and zona occludens-1 (ZO-1) in hCMEC/D3 cells following treatment for
859 24 h with 1 μ M propionate, with or without inclusion of 50 ng/ml LPS for the last 12 h
860 of incubation. Scale bar (10 μ m) applies to all images. Images are representative of at
861 least three independent experiments. (d) Expression of *CD14* mRNA in control and
862 propionate-treated (1 μ M; 24 h) hCMEC/D3 cells according to microarray data (data
863 are mean \pm SEM, $n = 3$). (e) Surface expression of CD14 protein on control and
864 propionate-treated hCMEC/D3 cells (grey line, unstained cells, black line secondary
865 antibody control, red line FFAR3), data are representative of three independent
866 experiments. (f) Median fluorescence intensity of surface expression of CD14 protein
867 on control and propionate-treated hCMEC/D3 cells, dashed line indicates isotype
868 control fluorescence intensity; data are mean \pm SEM, $n=3$ independent experiments.

869

870 **Fig. 3:** Protective effects of propionate against oxidative stress. (a) Representation of
871 stress-response genes significantly upregulated in the current study and directly
872 influenced by NFE2L2, '*the master regulator of antioxidant responses*' [54]. (b)
873 Confocal microscopic analysis of expression of NFE2L2 (Nrf2) in hCMEC/D3 cells
874 following treatment for 24 h with 1 μ M propionate; scale bar (10 μ m) applies to all
875 images. Images are representative of at least three independent experiments. (c)
876 Production of reactive oxygen species (ROS) in control and propionate pre-treated (1
877 μ M, 24 h) hCMEC/D3 cells treated for 30 min with the mitochondrial complex I inhibitor
878 rotenone (2.5 μ M). Data are mean \pm SEM, $n=3$ independent experiments.

879

880 **Fig. 4:** Production of propionate by the human gut microbiota. Propionate can be
881 produced directly or indirectly by cross-feeding from succinate- and lactate-producers
882 (e.g. *Selenomonas*, *Megasphaera* and *Veillonella* spp.). Image produced using
883 information taken from [57]. **Akkermansia muciniphila* is known to produce
884 propionate; it is thought to do this via the succinate pathway [57].

885

886 **Supplementary Fig. 1:** Persistence of the protective effect of propionate upon LPS-
887 induced barrier disruption across different doses. (a) Assessment of the paracellular
888 permeability of hCMEC/D3 monolayers to 70 kDa FITC-dextran following treatment
889 for 24 h with 1, 10 or 100 μ M propionate, with or without inclusion of 50 ng/ml LPS for
890 the last 12 h of incubation; data are mean \pm SEM, $n = 3$ independent experiments. (b)
891 Trans-endothelial electrical resistance of hCMEC/D3 monolayers following treatment
892 for 24 h with 1, 10 or 100 μ M propionate, with or without inclusion of 50 ng/ml LPS for
893 the last 12 h of incubation; data are mean \pm SEM, $n = 3$ independent experiments.

894

895 **Supplementary Fig. 2:** Protective effects of propionate against LPS-induced barrier
896 disruption in primary human brain microvascular endothelial cells (HBMEC). (a)
897 Assessment of the paracellular permeability of HBMEC monolayers to 70 kDa FITC-
898 dextran following treatment for 24 h with 1 μ M propionate, with or without inclusion of
899 50 ng/ml LPS for the last 12 h of incubation; data are mean \pm SEM, $n = 3$ independent
900 experiments. (b) Trans-endothelial electrical resistance of HBMEC monolayers
901 following treatment for 24 h with 1 μ M propionate, with or without inclusion of 50 ng/ml
902 LPS for the last 12 h of incubation; data are mean \pm SEM, $n = 3$ independent
903 experiments.

904

905 **Supplementary Fig. 3:** Effects of propionate upon expression and activity of typical
906 cerebrovascular efflux transporter systems. (a) Surface expression of BCRP,
907 LRP-1 and P-glycoprotein on control and propionate-treated (1 μ M, 24 h) hCMEC/D3
908 cells (black, control, red, propionate), data are representative of three independent
909 experiments. (b) Median fluorescence intensity of surface expression of BCRP, LRP-
910 1 and P-glycoprotein on control and propionate-treated (1 μ M, 24 h) hCMEC/D3 cells;
911 data are mean \pm SEM, $n=3$ independent experiments. (c) Lack of stimulatory effect of
912 propionate upon BCRP, data are mean \pm SEM, $n = 4$. (d) Lack of inhibitory effect of
913 propionate upon stimulated ATP-dependent activity of BCRP, data are mean \pm SEM,
914 $n = 4$. (e) Lack of stimulatory effect of propionate upon P-glycoprotein, data are mean
915 \pm SEM, $n = 4$. (f) Lack of inhibitory effect of propionate upon stimulated ATP-dependent
916 activity of P-glycoprotein, data are mean \pm SEM, $n = 4$.

917

918

919 **Supplementary Table 1:** Effects of propionate treatment (1 μ M, 24 h) upon mRNA
920 expression of BBB-related genes in hCMEC/D3 cells, grouped in broad functional
921 categories. Gene names listed in bold were significantly regulated compared to
922 untreated cells ($P_{\text{FDR}} < 0.05$)

923

924 **Supplementary Table 2:** Effects of propionate treatment (1 μ M, 24 h) upon mRNA
925 expression of antioxidant system-related genes in hCMEC/D3 cells. Gene names
926 listed in bold were significantly regulated compared to untreated cells ($P_{\text{FDR}} < 0.05$).

927

Figure 1

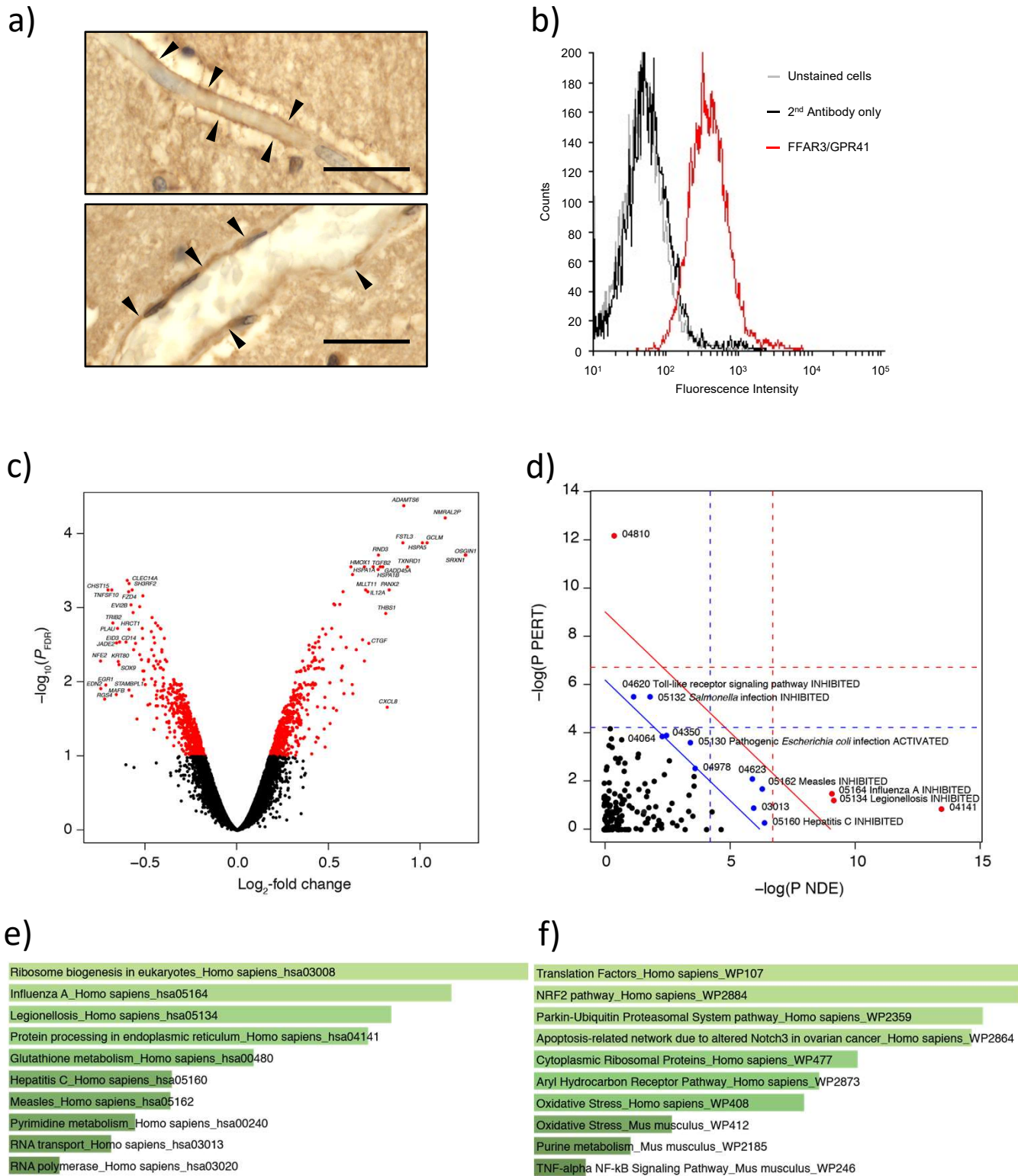


Figure 2

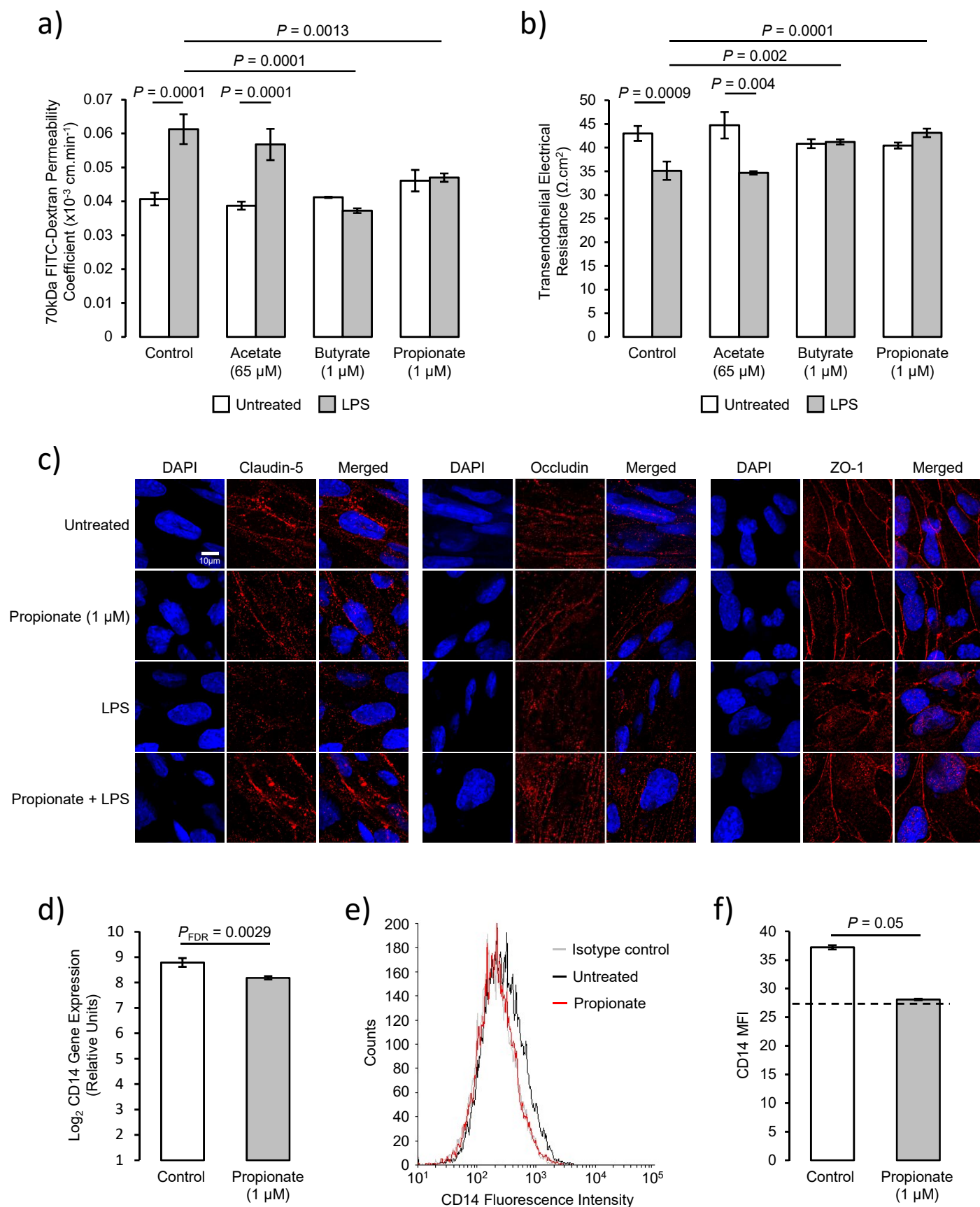


Figure 3

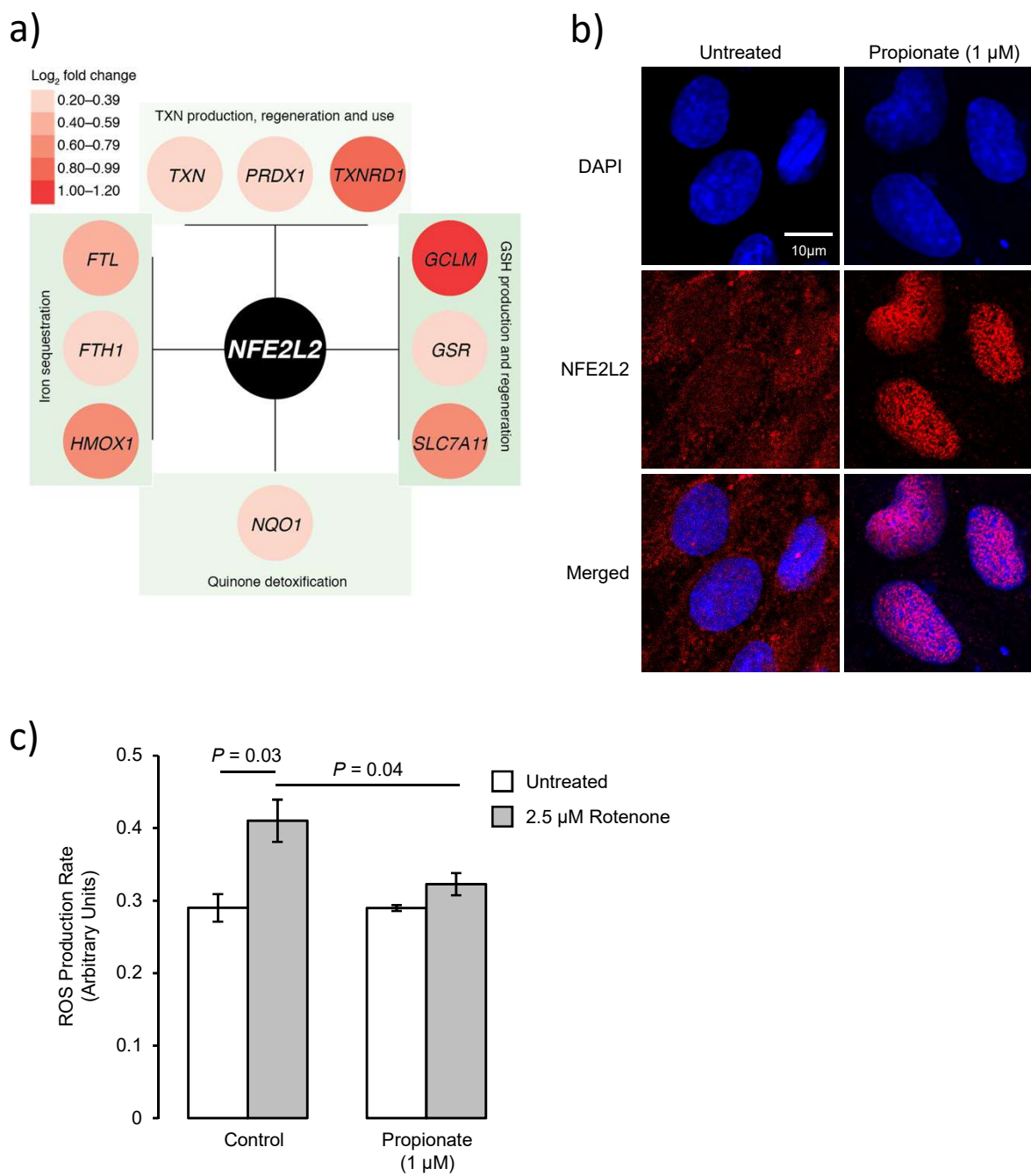
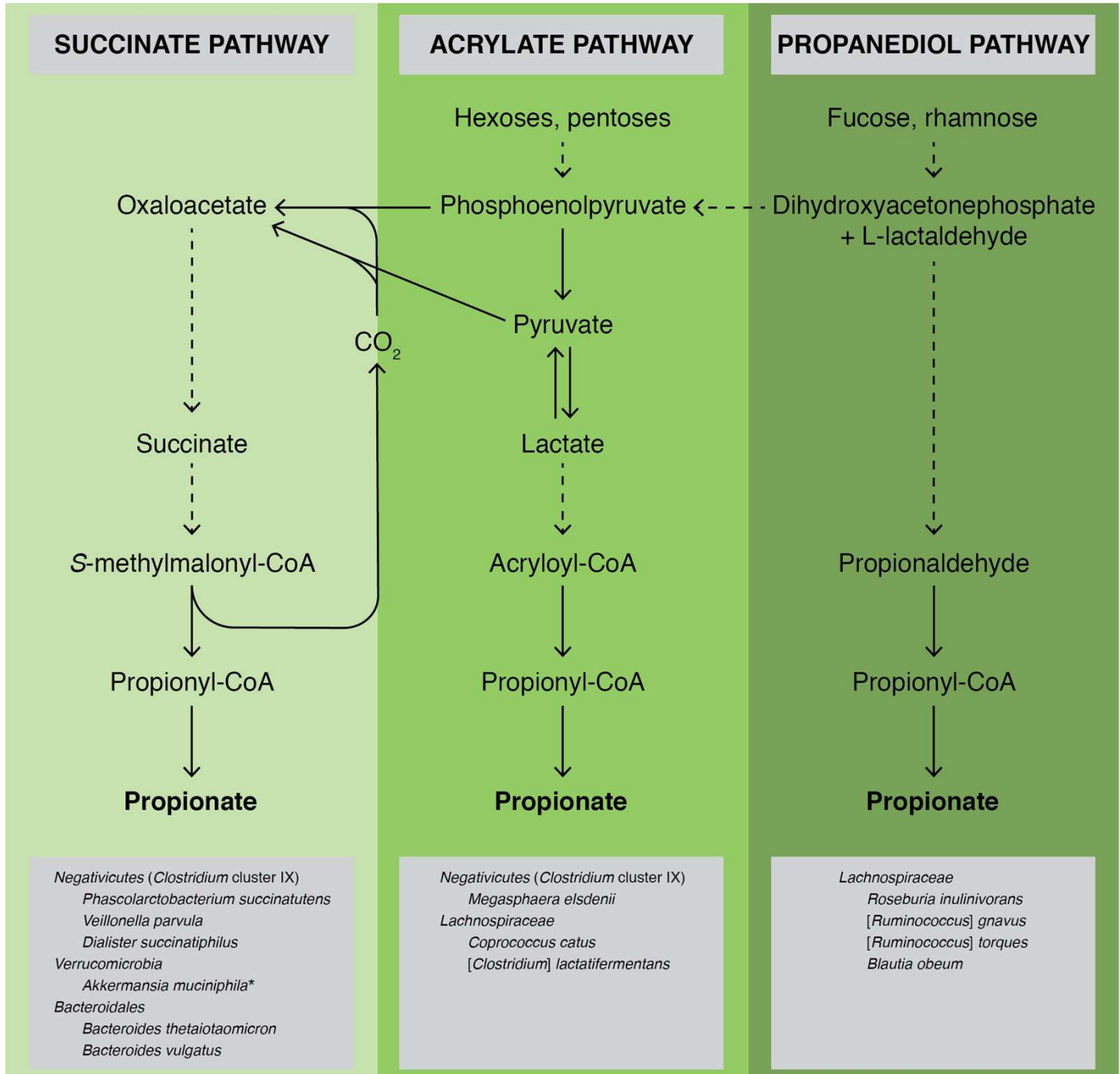
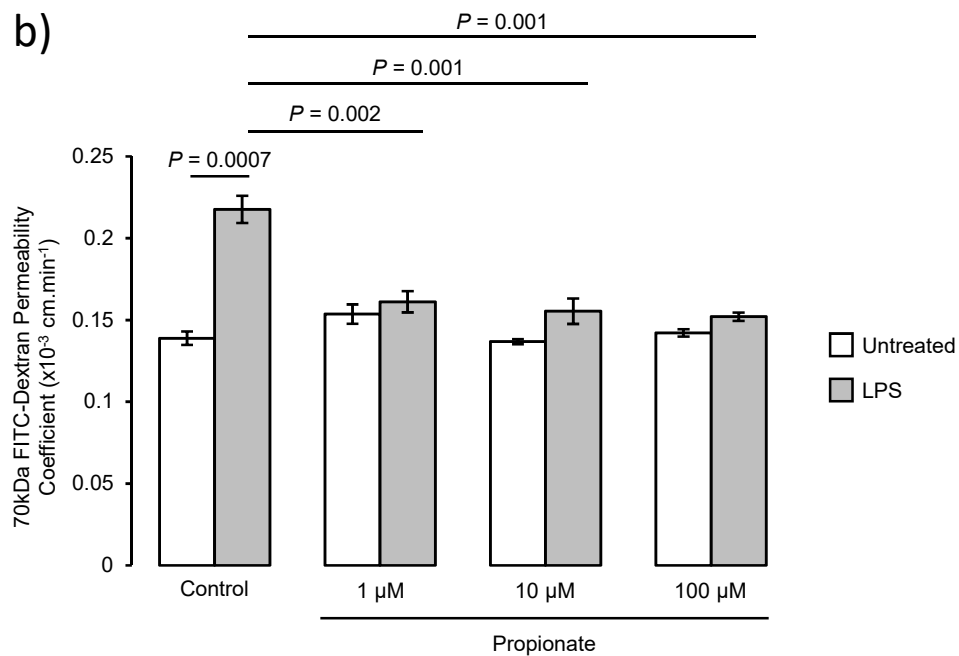
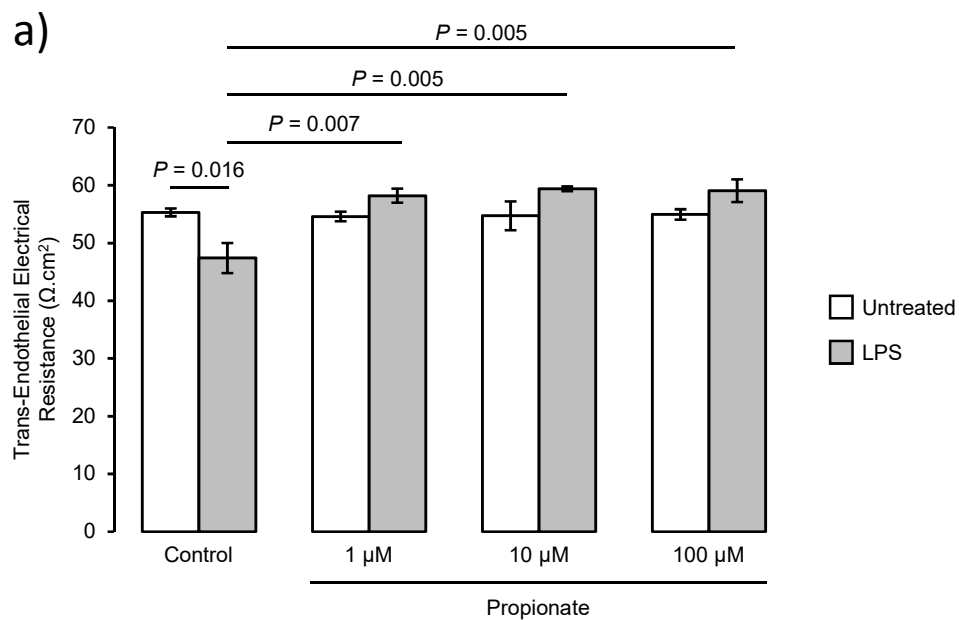


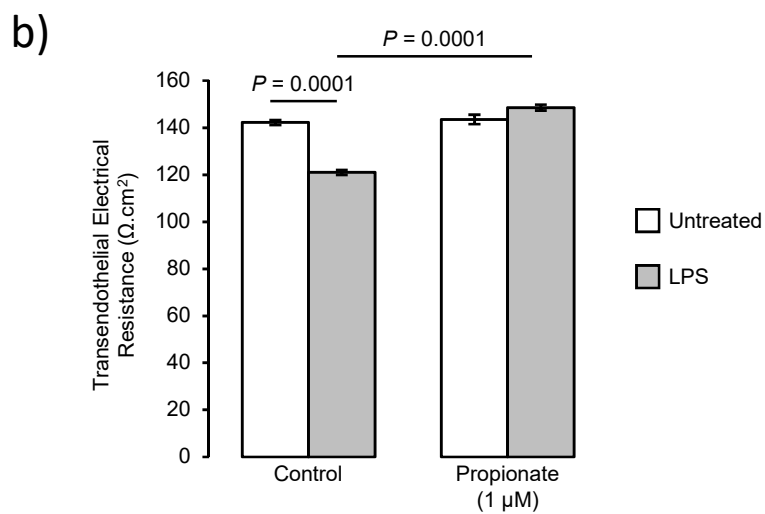
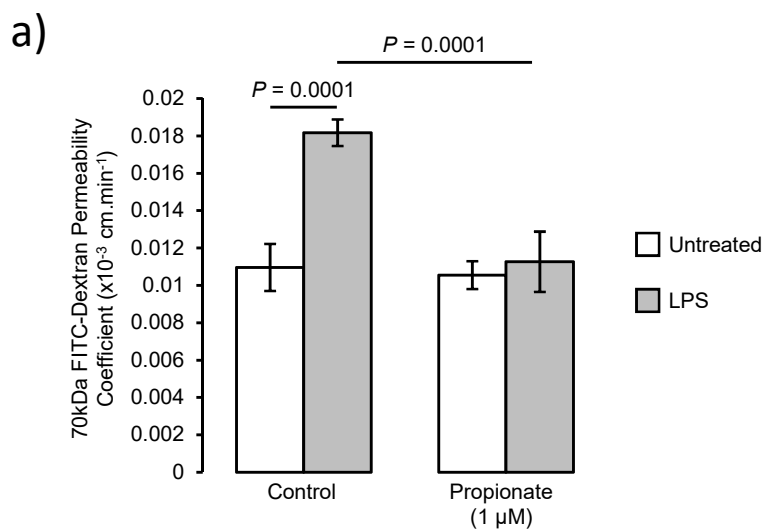
Figure 4



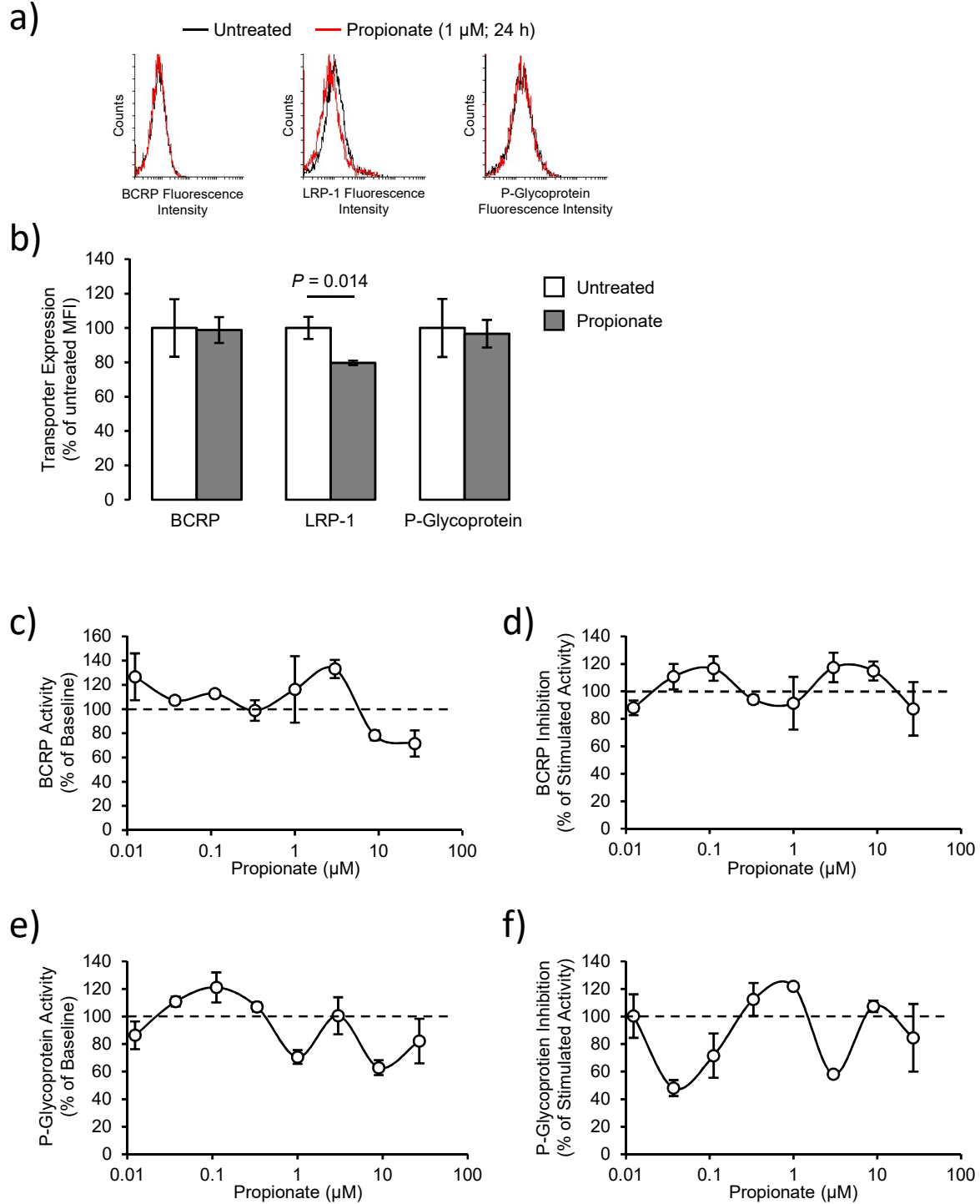
Supplementary Figure 1



Supplementary Figure 2



Supplementary Figure 3



Cell Adhesion/Junctional proteins/Cytoskeletal factors

<u>Symbol</u>	<u>Description</u>	<u>logFC</u>	<u>adj.P.Val</u>
PECAM1	platelet and endothelial cell adhesion molecule 1	-0.518	0.002
CLDN11	claudin 11	0.541	0.024
GJA1	gap junction protein alpha 1	0.434	0.055
CLDN1	claudin 1	0.264	0.062
JAM3	junctional adhesion molecule 3	0.180	0.132
UTRN	utrophin	-0.155	0.157
CDH2	cadherin 2	0.167	0.184
CLDN7	claudin 7	-0.122	0.270
ANXA1	annexin A1	0.145	0.270
TJP2	tight junction protein 2	-0.124	0.281
CLDN17	claudin 17	-0.124	0.282
CLDN4	claudin 4	0.141	0.341
SMARCA2	SWI/SNF related, matrix associated, actin dependent regulator of chromatin, subfamily a, member 2	0.118	0.373
CLDN23	claudin 23	-0.108	0.462
JAM2	junctional adhesion molecule 2	-0.110	0.540
TJP1	tight junction protein 1	0.090	0.573
CLDN6	claudin 6	0.092	0.582
LAMA4	laminin subunit alpha 4	-0.078	0.629
LAMA3	laminin subunit alpha 3	-0.070	0.657
DAG1	dystroglycan 1	-0.067	0.663
CLDN20	claudin 20	0.073	0.666
AGRN	agrin	0.055	0.694
CLDN12	claudin 12	0.064	0.751
CLDN8	claudin 8	-0.049	0.753
CLDN15	claudin 15	-0.050	0.778
CTNNB1	catenin beta 1	-0.047	0.783
VIM	vimentin	0.041	0.792
HAPLN2	hyaluronan and proteoglycan link protein 2	-0.054	0.794
DTNA	dystrobrevin alpha	0.053	0.796
ESAM	endothelial cell adhesion molecule	-0.043	0.799
LAMB2	laminin subunit beta 2	-0.044	0.803
CLDN9	claudin 9	-0.039	0.804
LAMA2	laminin subunit alpha 2	-0.057	0.808
ITM2A	integral membrane protein 2A	-0.041	0.837
FN1	fibronectin 1	-0.037	0.852
COL4A1	collagen type IV alpha 1 chain	0.030	0.875
TJP3	tight junction protein 3	-0.027	0.894
CLDN3	claudin 3	-0.023	0.906
GJB6	gap junction protein beta 6	0.022	0.911
CDH5	cadherin 5	-0.029	0.920
LAMA1	laminin subunit alpha 1	0.014	0.948
CLDN5	claudin 5	-0.016	0.962
CLDN22	claudin 22	0.013	0.963
ACTB	actin beta	0.009	0.965
CLDN10	claudin 10	-0.009	0.966
ADGRA2	adhesion G protein-coupled receptor A2	0.010	0.966
ITGA3	integrin subunit alpha 3	-0.009	0.967

OCLN	occludin	-0.007	0.969
HSPG2	heparan sulfate proteoglycan 2	0.008	0.973
DMD	dystrophin	-0.003	0.989
AFDN	afadin, adherens junction formation factor	0.003	0.989
MARVELD2	MARVEL domain containing 2	-0.001	0.996

Transporter proteins

<u>Symbol</u>	<u>Description</u>	<u>logFC</u>	<u>adj.P.Val</u>
SLC1A5	solute carrier family 1 member 5	0.400	0.011
SLC44A1	solute carrier family 44 member 1	-0.261	0.030
SLC7A5	solute carrier family 7 member 5	0.206	0.092
TFRC	transferrin receptor	0.262	0.099
SLC38A5	solute carrier family 38 member 5	0.194	0.165
SLC38A3	solute carrier family 38 member 3	0.140	0.240
SLC22A5	solute carrier family 22 member 5	0.140	0.272
SLC29A4	solute carrier family 29 member 4	0.144	0.299
SLC22A8	solute carrier family 22 member 8	-0.126	0.308
SLC2A1	solute carrier family 2 member 1	-0.129	0.342
SLC38A2	solute carrier family 38 member 2	0.120	0.381
SLC28A2	solute carrier family 28 member 2	0.133	0.411
SLC5A1	solute carrier family 5 member 1	0.100	0.447
SLC5A6	solute carrier family 5 member 6	0.094	0.452
SLC6A6	solute carrier family 6 member 6	0.096	0.461
SLC1A4	solute carrier family 1 member 4	-0.115	0.462
SLC27A4	solute carrier family 27 member 4	-0.139	0.463
LRP2	LDL receptor related protein 2	0.082	0.501
SLC38A1	solute carrier family 38 member 1	0.091	0.510
SLC22A1	solute carrier family 22 member 1	0.078	0.560
LDLR	low density lipoprotein receptor	-0.075	0.566
SLC1A3	solute carrier family 1 member 3	0.084	0.581
MFSD2A	major facilitator superfamily domain containing 2A	0.079	0.593
ABCG2	ATP binding cassette subfamily G member 2 (Junior blood group)	0.066	0.671
INSR	insulin receptor	0.060	0.718
AQP4	aquaporin 4	0.060	0.733
SLC16A2	solute carrier family 16 member 2	-0.057	0.780
ABCC5	ATP binding cassette subfamily C member 5	-0.041	0.793
SLCO1C1	solute carrier organic anion transporter family member 1C1	0.041	0.795
SLC29A1	solute carrier family 29 member 1 (Augustine blood group)	0.036	0.807
SLC27A1	solute carrier family 27 member 1	-0.036	0.818
SLC7A3	solute carrier family 7 member 3	0.038	0.824
SLC22A2	solute carrier family 22 member 2	0.035	0.843
SLC16A1	solute carrier family 16 member 1	-0.047	0.847
ABCB1	ATP binding cassette subfamily B member 1	0.029	0.866
AGER	advanced glycosylation end-product specific receptor	-0.026	0.908
AVPR1A	arginine vasopressin receptor 1A	-0.023	0.912
ABCA2	ATP binding cassette subfamily A member 2	0.015	0.947
SLC6A9	solute carrier family 6 member 9	0.013	0.949
SLC1A1	solute carrier family 1 member 1	-0.013	0.954
SLC7A1	solute carrier family 7 member 1	0.013	0.955
ABCC1	ATP binding cassette subfamily C member 1	0.012	0.956

SLC22A3	solute carrier family 22 member 3	-0.012	0.957
LEPR	leptin receptor	-0.009	0.960
SLC16A7	solute carrier family 16 member 7	-0.012	0.962
ABCC4	ATP binding cassette subfamily C member 4	-0.011	0.963
SLC5A3	solute carrier family 5 member 3	-0.009	0.967
SLC7A6	solute carrier family 7 member 6	-0.008	0.969
SLCO2B1	solute carrier organic anion transporter family member 2B1	-0.005	0.983
ABCC2	ATP binding cassette subfamily C member 2	-0.003	0.988
SLCO1B1	solute carrier organic anion transporter family member 1B1	0.003	0.988
SLC2A13	solute carrier family 2 member 13	0.003	0.990
SLC1A2	solute carrier family 1 member 2	0.001	0.995

Inflammatory response

<u>Symbol</u>	<u>Description</u>	<u>logFC</u>	<u>adj.P.Val</u>
TNFSF10	tumor necrosis factor superfamily member 10	-0.684	0.001
PDGFRB	platelet derived growth factor receptor beta	-0.441	0.015
TNFRSF1A	TNF receptor superfamily member 1A	-0.289	0.021
TNFRSF12A	TNF receptor superfamily member 12A	0.383	0.028
TNFRSF21	TNF receptor superfamily member 21	0.325	0.031
ITGB4	integrin subunit beta 4	-0.205	0.056
TNFAIP6	TNF alpha induced protein 6	0.325	0.118
PODXL	podocalyxin like	-0.194	0.130
ITGA5	integrin subunit alpha 5	-0.211	0.163
ITGA1	integrin subunit alpha 1	-0.150	0.188
PTGS2	prostaglandin-endoperoxide synthase 2	0.187	0.189
ITGB5	integrin subunit beta 5	-0.156	0.193
CXCL2	C-X-C motif chemokine ligand 2	0.171	0.231
IKBKB	inhibitor of nuclear factor kappa B kinase subunit beta	-0.139	0.299
SOD1	superoxide dismutase 1, soluble	0.126	0.338
ITGB8	integrin subunit beta 8	-0.144	0.340
NOS1	nitric oxide synthase 1	0.114	0.366
CCR5	C-C motif chemokine receptor 5 (gene/pseudogene)	0.222	0.391
ITGA4	integrin subunit alpha 4	0.161	0.430
CLEC5A	C-type lectin domain family 5 member A	0.138	0.441
ITGA6	integrin subunit alpha 6	-0.092	0.442
GRN	granulin precursor	-0.089	0.455
MMP9	matrix metalloproteinase 9	-0.099	0.475
NR3C1	nuclear receptor subfamily 3 group C member 1	-0.085	0.496
CRH	corticotropin releasing hormone	-0.092	0.558
AGT	angiotensinogen	-0.091	0.594
PTGDS	prostaglandin D2 synthase	-0.097	0.596
NOX4	NADPH oxidase 4	0.070	0.601
MMP2	matrix metalloproteinase 2	-0.088	0.687
SELP	selectin P	-0.074	0.689
IL1RN	interleukin 1 receptor antagonist	0.060	0.692
CXCR3	C-X-C motif chemokine receptor 3	-0.060	0.711
F11R	F11 receptor	-0.089	0.741
TNFRSF1B	TNF receptor superfamily member 1B	-0.098	0.760
SEMA7A	semaphorin 7A (John Milton Hagen blood group)	0.054	0.770
ITGB3	integrin subunit beta 3	0.049	0.793

ITGAV	integrin subunit alpha V	-0.033	0.837
TLR2	toll like receptor 2	0.030	0.860
ITGB1	integrin subunit beta 1	0.026	0.880
PTGER3	prostaglandin E receptor 3	-0.022	0.895
TNF	tumor necrosis factor	-0.016	0.927
ITGB2	integrin subunit beta 2	-0.012	0.951
IL1B	interleukin 1 beta	-0.033	0.967
CCR2	C-C motif chemokine receptor 2	-0.007	0.970
CD276	CD276 molecule	0.006	0.973
C3	complement C3	-0.001	0.997

Vascular function/coagulation cascade

<u>Symbol</u>	<u>Description</u>	<u>logFC</u>	<u>adj.P.Val</u>
SERPINE2	serpin family E member 2	0.461	0.007
PROCR	protein C receptor	0.240	0.046
PLAT	plasminogen activator, tissue type	-0.242	0.051
SERPINE1	serpin family E member 1	0.244	0.212
PROS1	protein S (alpha)	-0.165	0.262
PROC	protein C, inactivator of coagulation factors Va and VIIIa	-0.128	0.479
CA1	carbonic anhydrase 1	0.081	0.518
VWF	von Willebrand factor	-0.139	0.567
AVP	arginine vasopressin	-0.057	0.758
SERPINI1	serpin family I member 1	-0.033	0.840
PLG	plasminogen	-0.030	0.884
KNG1	kininogen 1	-0.024	0.898
NOS3	nitric oxide synthase 3	0.037	0.905
MYLK	myosin light chain kinase	-0.014	0.949
PTAFR	platelet activating factor receptor	-0.013	0.952
EPAS1	endothelial PAS domain protein 1	0.010	0.955

Endothelial proliferation/angiogenesis

<u>Symbol</u>	<u>Description</u>	<u>logFC</u>	<u>adj.P.Val</u>
PDGFB	platelet derived growth factor subunit B	-0.226	0.090
TMEFF2	transmembrane protein with EGF like and two follistatin like domains 2	0.166	0.170
S100A12	S100 calcium binding protein A12	0.143	0.245
FGF19	fibroblast growth factor 19	-0.157	0.354
IGFBP3	insulin like growth factor binding protein 3	0.091	0.486
RGS5	regulator of G-protein signaling 5	-0.075	0.548
FLT1	fms related tyrosine kinase 1	-0.112	0.572
HNRNPDL	heterogeneous nuclear ribonucleoprotein D like	-0.084	0.601
VEGFA	vascular endothelial growth factor A	-0.072	0.617
S100B	S100 calcium binding protein B	-0.071	0.643
EZH1	enhancer of zeste 1 polycomb repressive complex 2 subunit	-0.068	0.722
PTPRB	protein tyrosine phosphatase, receptor type B	-0.057	0.745
HMGB1	high mobility group box 1	0.044	0.775
PTN	pleiotrophin	-0.029	0.920
KDR	kinase insert domain receptor	0.022	0.934
BTG2	BTG anti-proliferation factor 2	0.012	0.958
EPO	erythropoietin	-0.011	0.963

Other BBB-related genes

<u>Symbol</u>	<u>Description</u>	<u>logFC</u>	<u>adj.P.Val</u>
EPHA2	EPH receptor A2	-0.249	0.076
MOG	myelin oligodendrocyte glycoprotein	-0.090	0.546
CLN3	CLN3, battenin	-0.085	0.566
SRGN	serglycin	0.072	0.574
MBP	myelin basic protein	-0.066	0.646
RAMP2	receptor activity modifying protein 2	0.054	0.713
CLCN2	chloride voltage-gated channel 2	-0.055	0.733
CPE	carboxypeptidase E	0.044	0.811
CYBB	cytochrome b-245 beta chain	0.033	0.856
MPZL1	myelin protein zero like 1	0.028	0.864
GAB2	GRB2 associated binding protein 2	-0.030	0.866
MAP3K7	mitogen-activated protein kinase kinase kinase 7	0.028	0.882
APP	amyloid beta precursor protein	-0.044	0.890
APLP2	amyloid beta precursor like protein 2	0.022	0.914
PLP1	proteolipid protein 1	0.019	0.935
HDC	histidine decarboxylase	0.007	0.985
HRH3	histamine receptor H3	0.003	0.989
APOE	apolipoprotein E	0.000	1.000
GFAP	glial fibrillary acidic protein	0.000	1.000

Supplementary Table 2: Human anti-oxidant genes included in array analyses in this study

Symbol	log ₂ fold change	Adjusted <i>P</i> value	Synonyms	Description
GCLM†	1.034	1.312×10 ⁻⁴	GLCLR	glutamate-cysteine ligase modifier subunit
SRXN1	1.242	1.934×10 ⁻⁴	C20orf139, Npn3, SRX, SRX1	sulfiredoxin 1
TXNRD1*	0.928	2.770×10 ⁻⁴	GRIM-12, TR, TR1, TRXR1, TXNR	thioredoxin reductase 1
HMOX1†	0.693	2.770×10 ⁻⁴	HMOX1D, HO-1, HSP32, bK286B10	heme oxygenase 1
FTL†	0.564	2.467×10 ⁻³	LFTD, NBIA3	ferritin light chain
SLC7A11†	0.649	3.676×10 ⁻³	CCBR1, xCT	solute carrier family 7 member 11
TXNL4B	0.388	6.601×10 ⁻³	DLP, Dim2	thioredoxin like 4B
NQO1†	0.345	0.015	DHQU, DIA4, DTD, NMOR1, NMORI, QR1	NAD(P)H quinone dehydrogenase 1
TXNDC9	0.346	0.020	APACD, PHLP3	thioredoxin domain containing 9
PRDX1*	0.306	0.021	MSP23, NKEF-A, NKEFA, PAG, PAGA, PAGB, PRX1, PRXI, TDPX2	peroxiredoxin 1
MT1F	-0.254	0.039	MT1	metallothionein 1F
MT1G	0.224	0.043	MT1, MT1K	metallothionein 1G
GLRX3	0.256	0.045	GLRX4, GRX3, GRX4, PICOT, TXNL2, TXNL3	glutaredoxin 3
TXN*	0.240	0.050	TRDX, TRX, TRX1	thioredoxin
FTH1†	0.206	0.061	FHC, FTH, FTHL6, HFE5, PIG15, PLIF	ferritin heavy chain 1
GSR*	0.328	0.061	HEL-75, HEL-S-122m	glutathione-disulfide reductase
MSRA	-0.222	0.082	PMSR	methionine sulfoxide reductase A
TXNDC5	0.217	0.085	ENDOPDI, ERP46, HCC-2, HCC2, PDIA15, STRF8, UNQ364	thioredoxin domain containing 5
MT1M	-0.213	0.106	MT-1M, MT-IM, MT1, MT1K	metallothionein 1M
GPX7	0.210	0.110	CL683, GPX6, GPx-7, GSHPx-7, NPGPx	glutathione peroxidase 7
TXNRD2	-0.166	0.164	SELZ, TR, TR-BETA, TR3, TRXR2	thioredoxin reductase 2
ERP44	0.170	0.165	PDIA10, TXNDC4	endoplasmic reticulum protein 44
PRDX4	0.153	0.173	AOE37-2, AOE372, HEL-S-97n, PRX-4	peroxiredoxin 4
SOD2	0.191	0.238	IPO-B, IPOB, MNSOD, MVCD6, Mn-SOD	superoxide dismutase 2, mitochondrial
PDIA6	0.132	0.250	ERP5, P5, TXNDC7	protein disulfide isomerase family A member 6
TXNDC8	-0.176	0.262	SPTRX-3, TRX6, bA427L11.2	thioredoxin domain containing 8
GPX4	-0.125	0.315	GPx-4, GSHPx-4, MCSP, PHGPx, SMDS, snGPx, snPHGPx	glutathione peroxidase 4
SOD1	0.126	0.338	ALS, ALS1, HEL-S-44, IPOA, SOD, hSod1, homodimer	superoxide dismutase 1, soluble

Symbol	log ₂ fold change	Adjusted P value	Synonyms	Description
TMX1	0.140	0.354	PDIA11, TMX, TXNDC, TXNDC1	thioredoxin related transmembrane protein 1
GLRX	-0.110	0.375	GRX, GRX1	glutaredoxin
TXNDC17	0.111	0.404	TRP14, TXNL5	thioredoxin domain containing 17
MT1A	-0.096	0.479	MT1, MT1S, MTC	metallothionein 1A
PRDX3	0.084	0.486	AOP-1, AOP1, HBC189, MER5, PRO1748, SP-22, prx-III	peroxiredoxin 3
GLRX2	0.086	0.500	CGI-133, GRX2	glutaredoxin 2
NME9	0.093	0.506	NM23-H9, TXL-2, TXL2, TXNDC6	NME/NM23 family member 9
TXNDC12	0.114	0.539	AG1, AGR1, ERP16, ERP18, ERP19, PDIA16, TLP19, hAG-1, hTLP19	thioredoxin domain containing 12
MT1X	0.104	0.544	MT-1I, MT1	metallothionein 1X
PRDX6	0.081	0.549	1-Cys, AOP2, HEL-S-128m, NSGPx, PRX, aiPLA2, p29	peroxiredoxin 6
GPX6	-0.087	0.567	GPX5p, GPXP3, GPx-6, GSHPx-6, dJ1186N24, dJ1186N24.1	glutathione peroxidase 6
GPX3	-0.073	0.622	GPx-P, GSHPx-3, GSHPx-P	glutathione peroxidase 3
TMX2	0.063	0.637	CGI-31, PDIA12, PIG26, TXNDC14	thioredoxin related transmembrane protein 2
CAT	0.068	0.642	-	catalase
PRDX5	-0.064	0.662	ACR1, AOEB166, B166, HEL-S-55, PLP, PMP20, PRDX6, PRXV, SBBI10, prx-V	peroxiredoxin 5
MT1E	-0.091	0.687	MT-1E, MT-IE, MT1, MTD	metallothionein 1E
GPX5	0.053	0.694	HEL-S-75p	glutathione peroxidase 5
GPX1	-0.059	0.698	GPXD, GSHPX1	glutathione peroxidase 1
SOD3	-0.048	0.763	EC-SOD	superoxide dismutase 3, extracellular
GLRX5	-0.047	0.777	C14orf87, FLB4739, GRX5, PR01238, PRO1238, PRSA, SIDBA3, SPAHGCG	glutaredoxin 5
SELENOP	0.040	0.794	SELP, SEPP, SEPP1, SeP	selenoprotein P
TXN2	0.052	0.832	COXPD29, MT-TRX, MTRX, TRX2	thioredoxin 2
CCS	-0.031	0.841	-	copper chaperone for superoxide dismutase
MT1H	0.041	0.853	MT-0, MT-1H, MT-IH, MT1	metallothionein 1H
CP	0.023	0.889	CP-2	ceruloplasmin
TXNIP	0.151	0.899	ARRDC6, EST01027, HHCPA78, THIF, VDUP1	thioredoxin interacting protein
TXNDC11	-0.021	0.907	EFP1	thioredoxin domain containing 11
PRDX2	0.016	0.935	HEL-S-2a, NKEF-B, NKEFB, PRP, PRX2, PRXII, PTX1, TDPX1, TPX1, TSA	peroxiredoxin 2
MT2A	-0.014	0.942	MT2	metallothionein 2A
NME8	-0.015	0.943	CILD6, HEL-S-99, NM23-H8, SPTRX2, TXNDC3, sptrx-2	NME/NM23 family member 8
TXNDC2	-0.012	0.953	SPTRX, SPTRX1	thioredoxin domain containing 2

Symbol	log ₂ fold change	Adjusted P value	Synonyms	Description
TMX4	-0.011	0.961	DJ971N18.2, PDIA14, TXNDC13	thioredoxin related transmembrane protein 4
MT1B	-0.009	0.963	MT-1B, MT-IB, MT1, MT1Q, MTP	metallothionein 1B
TXNL1	-0.013	0.968	HEL-S-114, TRP32, TXL-1, TXNL, TxI	thioredoxin like 1
GPX2	-0.008	0.969	GI-GPx, GPRP, GPRP-2, GPx-2, GPx-GI, GSHPX-GI, GSHPx-2	glutathione peroxidase 2
TMX3	-0.007	0.982	PDIA13, TXNDC10	thioredoxin related transmembrane protein 3

†Anti-oxidant genes identified from Enrichr search and Gorrini *et al.* (2013), and included in **Fig. 3a**.

*Anti-oxidant genes identified from Enrichr search, Gorrini *et al.* (2013) and Gelain *et al.* (2009), and included in **Fig. 3a**.